HHS Public Access

Author manuscript

FASEB J. Author manuscript; available in PMC 2024 May 08.

Published in final edited form as:

FASEB J. 2023 August ; 37(8): e23100. doi:10.1096/fj.202300757R.

Lethal eosinophilic crystalline pneumonia in mice expressing a stabilized *Csf2* mRNA

Yukitomo Arao[1], **Deborah J. Stumpo**[1], **Mark J. Hoenerhoff**[2], **Robert M. Tighe**[3], **Yen-Rei Yu**[4], **Deloris Sutton**[5], **Amogh Kashyap**[6], **Isabel Beerman**[6], **Perry J. Blackshear**[1,7,8]

[1] Signal Transduction Laboratory, National Institute of Environmental Health Sciences/NIH, Durham, NC 27709

[2] In Vivo Animal Core, Unit for Laboratory Animal Medicine, University of Michigan, Ann Arbor, MI 48109

[3] Division of Pulmonary, Allergy, and Critical Medicine, Department of Medicine, Duke University School of Medicine, Durham, NC 27710

[4] Division of Pulmonary Sciences and Critical Care Medicine, Department of Medicine, University of Colorado Anschutz Medical Campus, Aurora, CO 80045

[5] Cellular & Molecular Pathology Branch, National Institute of Environmental Health Sciences/ NIH, Durham, NC 27709

[6] Epigenetics and Stem Cell Aging Unit, National Institute on Aging/ NIH, Baltimore, MD 21224

[7] Departments of Medicine and Biochemistry, Duke University Medical Center, Durham, NC 27710

Abstract

Granulocyte-macrophage colony-stimulating factor (GM-CSF) is a cytokine that stimulates the proliferation and differentiation of granulocyte and macrophage precursors. The mouse gene encoding GM-CSF, *Csf2*, is regulated at both transcriptional and post-transcriptional levels. An adenine-uridine rich element (ARE) within the 3'-untranslated region of *Csf2* mRNA was shown in cell transfection studies to confer instability on this transcript. To explore the physiological importance of this element in an intact animal, we generated mice with a knock-in deletion of the 75 nucleotide ARE. Mice heterozygous for this ARE deletion developed severe respiratory distress and death within about 12 weeks of age. There was dense infiltration of lung alveolar spaces by crystal-containing macrophages. Increased stability of *Csf2* mRNA was confirmed in bone marrow-derived macrophages, and elevated GM-CSF levels were observed in serum and lung. These mice did not exhibit notable abnormalities in blood or bone marrow, and transplantation of

[8] To whom correspondence should be addressed: Perry J. Blackshear, 111 T.W. Alexander Dr., Durham, NC 27709, USA; black009@niehs.nih.gov.

Author contributions

YA, DJS and PJB designed the research studies, YA, DJS, Y-RY, DS, and AK were involved in conducting experiments and acquiring data, YA, DJS, MJH, RMT, Y-RY, DS, AK, IB, and PJB were involved in analyzing data, and YA, DJS and PJB were involved in writing the manuscript.

Conflict of interest statement

The authors declare that they have no conflicts of interest.

bone marrow from mutant mice into lethally irradiated WT mice did not confer the pulmonary phenotype. Mice with a conditional deletion of the ARE restricted to lung type II alveolar cells exhibited an essentially identical lethal lung phenotype at the same ages as the mice with the whole-body deletion. In contrast, mice with the same conditional ARE deletion in myeloid cells, including macrophages, exhibited lesser degrees of macrophage infiltration into alveolar spaces much later in life, at approximately 9 months of age. Post-transcriptional *Csf2* mRNA stability regulation in pulmonary alveolar epithelial cells appears to be essential for normal physiological GM-CSF secretion and pulmonary macrophage homeostasis.

Keywords

GM-CSF; mRNA stability; 3'-untranslated region; AU-rich element; alveolar macrophage; eosinophilic crystalline pneumonia

Introduction

Granulocyte-macrophage colony-stimulating factor (GM-CSF) is a small glycoprotein whose gene structure and protein sequence are highly conserved among mammals. GM-CSF was initially isolated as a potent hematopoietic regulatory protein capable of stimulating the proliferation and differentiation of granulocyte and macrophage precursors (1, 2). Physiological roles of GM-CSF have been analyzed using *Csf2* knock-out (KO) mice (3–7). In general, these mice do not exhibit abnormalities in steady-state hematopoiesis. However, they develop pulmonary disease characterized by the accumulation of surfactant proteins and phospholipids in alveolar spaces that is reminiscent of human pulmonary alveolar proteinosis (PAP) (3, 4). Several lines of evidence have suggested that GM-CSF is required for the proper regulation of pulmonary surfactant homeostasis, apparently through the enhancement of surfactant clearance by alveolar macrophages (AM) (8–10).

The expression of GM-CSF, encoded by the *CSF2* gene in humans and *Csf2* in mice, is regulated by various factors related to inflammation, such as tumor necrosis factor α (TNF) and interleukin-1 (11). The expression level of the *CSF2* transcript is tightly regulated by both transcriptional and post-transcriptional mechanisms (12–15). The importance of post-transcriptional regulation of GM-CSF mRNA turnover in the regulation of *CSF2* gene expression has been well documented (12, 15). Shaw and Kamen described a characteristic adenine and uridine-rich element (ARE) in the 3'-untranslated region (UTR) of the human *CSF2* mRNA (15), and showed that it conferred instability on the mRNA. The insertion of the *CSF2* mRNA ARE into the 3'-UTR of a stable mRNA, such as rabbit β-globin mRNA, resulted in a highly unstable transcript (15, 16), suggesting that this ARE promoted mRNA degradation. Since those initial findings, ARE-dependent regulation of mRNA turnover has been found in transcripts encoding many cytokines and inflammatory mediators (17, 18).

However, the contribution of this mRNA instability element in the *CSF2* mRNA to the physiology of an intact mammal has not been explored. To address this question, we generated a new knock-in (KI) mouse model in which the ARE instability element was deleted in the *Csf2* mRNA (GM-CSFΔARE). Whole body heterozygous GM-CSFΔARE mice exhibited respiratory distress and 100% mortality, with a median survival of

approximately 13 weeks of age. This lethal phenotype was associated with profound accumulations of macrophages in the alveolar spaces. We did not attempt to breed to homozygosity because of the severity and early onset of the phenotype. Deletion of the ARE on one allele increased the apparent stability of *Csf2* mRNA in bone marrow-derived macrophages isolated from GM-CSFΔARE mice. Elevated levels of GM-CSF protein were confirmed in serum and lung. Surprisingly, there were no other apparent morphological abnormalities of tissues in these mice at the time of death. This macrophage-infiltrating pneumonia phenotype was not recapitulated by transplantation of GM-CSFΔARE hematopoietic stem cells into lethally irradiated wild-type (WT) mice, excluding an important hematopoietic contribution to the phenotype. In contrast, mice that were either heterozygous or homozygous for a conditional GM-CSFΔARE deletion in pulmonary alveolar type II (AT2) cells exhibited a nearly identical, lethal form of pneumonia. These results demonstrate that the post-transcriptional regulation of *Csf2* expression in pulmonary AT2 cells is essential for normal pulmonary alveolar macrophage homeostasis. This GM-CSFΔARE mouse model illuminates an important and previously uncharacterized aspect of *Csf2* mRNA turnover regulation in balancing appropriate expression levels and regulating physiological responses.

Materials and Methods

Generation and use of GM-CSFΔARE mice

Conditional knock-in mice expressing a 75 bp AU-rich element (ARE)-deleted *Csf2* mRNA, termed GM-CSFΔARE, were generated by Ozgene Pty Ltd (Australia) using standard embryonic stem (ES) cell targeting techniques (deleted bases were 920–994 of GenBank accession number NM_009969.4; red text in Figure 1A). The targeting construct was generated from C57BL/6 mouse genomic DNA and cloned into the Ozgene PacF vector (Ozgene, Australia), containing PGK-neomycin flanked by Flp recombinase targeting sites (FRT). A 5’ homology arm contained *Csf2* exon 1 through exon 3, and the 5’-end LoxP flanked wild-type (WT) exon 4 encompassing the 75 bp ARE; a 3’ homology arm contained the 3’-end LoxP flanked 75 bp ARE-deleted mutant exon 4 (*Csf2* targeting vector; Figure 1B). All fragments in the targeting vector were generated by PCR and confirmed by restriction enzyme digestion and sequencing. C57BL/6 ES cells were electroporated with the AclI-linearized targeting vector. Correctly targeted ES cells were identified by Southern blot analysis using a 5’ probe with a BamHI-digested genomic DNA, and a 3’ probe with a NdeI-digested genomic DNA. Both probes bind outside the targeting vector sequence. A *neo* probe was used with HindIII, KpnI, NsiI, or SpeI-digested genomic DNA to exclude random integration clones. An endogenous probe (within the targeting vector) was used with ScaI-digested genomic DNA to identify the deletion of the PGK-neomycin selection cassette. Deletion of the PGK-neomycin cassette was performed at Ozgene through breeding with a Flp recombinase-expressing mouse. The resulting mice, which contained a LoxP sites-flanked WT *Csf2* exon 4 followed by a 75 bp deleted mutant exon 4, were referred to as $Csf2^{flARE/+}$ (X Flp mouse; Figure 1B). The $Csf2^{flARE/+}$ mice were crossed with Meox2-cre mice (B6.129S4-$Meox2^{tm1(cre)Sor}$/J; stock 003755, The Jackson Laboratory, Bar Harbor, ME) (19) to generate the knock-in mice containing only the mutant exon 4 (X Cre mouse; Figure 1B). Heterozygous $Csf2^{flARE/+}$ mice without Meox2-cre and WT ($Csf2^{+/+}$) mice with

or without Meox2-cre were used as control mice. Offspring were routinely genotyped by PCR using primer 1 (P1), 5'-TGG ACA GCG GAA GAC AAA CGA G-3' and primer 2 (P2), 5'-GCT TGT CCA CCA ACT CCA GAA GT C-3'. These primers amplified a 473 bp endogenous *Csf2* WT allele and a 398 bp Cre-mediated *Csf2* knock-in allele containing mutant exon 4. PCR conditions were: 93°C for 2 min then 30 cycles of 93°C for 30 sec, 58°C for 30 sec, and 72°C for 1 min with a final extension of 72°C for 10 min. Mice were also genotyped for the Meox2-cre using primers Meox2Cre common, 5'-GGG ACC ACC TTC TTT TGG CTT C-3', Meox2Cre WT, 5'-AAG ATG TGG AGA GTT CGG GGT AG-3', and Meox2Cre mutant, 5'-CCA GAT CCT CCT CAG AAA TCA GC-3'. These primers amplified a 410 bp WT allele and a 300 bp mutant (cre) allele. PCR conditions were as described by The Jackson Laboratory for the Meox2-cre mice.

To generate mice with an inducible *Csf2* ARE deletion in pulmonary alveolar type II (AT2) cells, the $Csf2^{flARE/+}$ mice were crossed with Sftpc-creER^{T2} mice (B6.129S-$Sftpc^{tm1(cre/ERT2)Blh}$/J; stock 028054, The Jackson Laboratory) (20) to generate $Csf2^{flARE/flARE}$ with or without Sftpc-creER^{T2}. Genotypes for this strain were analyzed by Transnetyx. To activate the *Sftpc* promoter-driven ER^{T2} fused cre recombinase, 0.1 mg/g body weight tamoxifen (MP Biomedicals, Solon, OH) dissolved in corn oil (Sigma-Aldrich, Inc., St. Louis, MO) was injected into the peritoneal cavity of male or female mice of 3–4 months of age for three consecutive days. Body weights of treated mice were monitored beginning every two weeks after the last tamoxifen injection.

To generate mice with a *Csf2* ARE deletion in myeloid cells, the $Csf2^{flARE/flARE}$ mice were crossed with LysM-cre mice (B6.129P2-$Lyz2^{tm1(cre)Ifo}$/J; stock 004781, The Jackson Laboratory) (21) to generate $Csf2^{flARE/flARE}$ mice with or without LysM-cre. All animal studies were conducted according to US Public Health Service Policy. All animal procedures used in this study except the bone marrow transplant studies were approved by the National Institute of Environmental Health Sciences Institutional Animal Care and Use Committee. The bone marrow transplant studies were approved by the National Institute on Aging Institutional Animal Care and Use Committee.

Histopathology and hematology

Most GM-CSFΔARE mice were euthanized between 5 and 16 weeks of age by carbon dioxide (CO_2) euthanasia; tissues were examined and fixed in 10% neutral buffered formalin and used for paraffin embedding, sectioning (5 μm sections), and staining with hematoxylin and eosin and/or for immunohistochemistry. Peripheral blood was collected by retro-orbital bleeding into EDTA-containing Microvette collection tubes (Sarstedt, Inc., Newton, NC) and analyzed using a Hemavet 1700 hematology analyzer (Drew Scientific, Inc., Miami Lakes, FL). For serum collection, peripheral blood was collected into Microvette collection tubes containing serum gel/clotting activator (Sarstedt, Inc.). After clotting, the tubes were centrifuged for 5 min at 10,000 × g, room temperature. Collected serum was stored at −80°C until it could be analyzed by ELISA.

Bronchoalveolar lavage (BAL) and peritoneal lavage fluid analysis

Mice at various ages were euthanized with an overdose of FatalPlus (sodium pentobarbital, Hospira, Inc., Lake Forest, IL), and lung lavage was performed with 2 × 1 ml of PBS containing 5 mM EDTA. Collected lavage fluid was centrifuged for 5 min at 500 × g, 4°C. The supernatants were stored at −80°C until they were analyzed by ELISA. Cell pellets were resuspended in PBS, either 0.5 ml for control or 1 ml for GM-CSFΔARE mice, and total cell counts were determined using a Countess Automated Cell Counter (Life Technologies, Grand Island, NY). BAL cells (5×10^4 cells) were prepared by Cytospin (Thermo Scientific) and stained with a modified Wright-Giemsa staining (HARLECO Hemacolor, EMD Chemicals, Inc., Gibbstown, NJ) for analyzing differential counts. Peritoneal cells were obtained after CO_2 euthanasia by peritoneal lavage using 5 ml PBS containing 5 mM EDTA. Peritoneal lavage fluid was centrifuged for 5 min at 500 × g, 4°C. Cell pellets were resuspended in 5 ml PBS; cell count determination, cytospin slide preparation, and staining were as described above.

Measurement of GM-CSF in serum, BAL fluid, and whole lung

Post-lavage lungs were homogenized in 2.0 ml (control) or 4.0 ml (GM-CSFΔARE) of PBS using a Tekmar Tissumizer. Homogenates were centrifuged at 10,000 × g for 5 min at 4°C to remove debris, and the supernatants were stored at −80°C until they were analyzed by ELISA. The concentrations of GM-CSF in serum, BAL supernatants, and post-lavage lung homogenates were measured by ELISA using the OptEIA mouse kit (BD Biosciences Pharmingen, San Diego, CA) according to the manufacturer's instructions. Absorbance at 450 nm was performed with the Tecan Infinite 200 Pro microplate reader (Tecan Group Ltd., Mannedorf, Switzerland) with a 570 nm wavelength set as reference.

Cytokine and chemokine analysis of serum and BAL fluid

Cytokines and chemokines were measured in serum and BAL fluid supernatants, prepared as described above, using a 25-plex Milliplex MAP mouse cytokine/chemokine magnetic bead panel (MilliporeSigma, Burlington, MA) on a Luminex-200 instrument (Luminex, Riverside, CA). Luminex XPonent 3.1 software (Luminex) was used for data analysis.

Isolation and culture of bone marrow-derived macrophages

Two- to 3 month-old mice were euthanized, and bone marrow cells were collected from both femurs, as described previously (22). Cells from one mouse were cultured overnight in T25 flasks in RPMI 1640 medium (Gibco-Life Technologies-Thermo Fisher Scientific, Waltham, MA) supplemented with 10% fetal bovine serum (FBS; Hyclone, Logan, UT), 25 mM HEPES, 2 mM glutamine, 100 U/ml penicillin, 100 μg/ml streptomycin (Life Technologies, Grand Island, NY), and 30% (v/v) L929 cell-conditioned medium. The following day, non-adherent cells were collected and cultured in 100 mm dishes in the same culture medium. Fresh culture medium was added to the plates every 3–4 days. Differentiated bone marrow-derived macrophages (BMDM) were obtained after 8–10 days in culture.

mRNA half-life analysis, isolation of RNA, and real-time PCR

mRNA decay studies were performed on serum-deprived BMDM. Cells were incubated overnight in RPMI 1640 medium (Gibco-Life Technologies-Thermo Fisher Scientific) supplemented with 1% FBS (Hyclone), glutamine, penicillin, and streptomycin. Cells were stimulated for 1 h with 1 μg/ml LPS (serotype 055:B5; Sigma-Aldrich, St. Louis, MO), followed by the addition of actinomycin D (Sigma-Aldrich) at a final concentration of 5 μg/ml. Cells were harvested at the indicated times after adding actinomycin D. Mouse tissues were collected into RNAlater (Thermo Fisher Scientific-Invitrogen-Applied Biosystems, Waltham, MA) following the manufacturer's instructions. Total cellular RNA was isolated from BMDM, the cells from BAL fluid, or mouse tissues by using the Illustra RNAspin kit (GE Healthcare Bio-Sciences, Pittsburgh, PA) following the manufacturer's instructions. Since very few BAL cells were present in the control mice, we pooled the collected cells from 5 control mice into one sample for RNA isolation. BAL cells from one GM-CSFΔARE mouse were enough to use for RNA isolation. RNA levels were determined by real-time RT-PCR. First-strand cDNAs were synthesized from the isolated RNA using oligo$(dT)_{12–18}$ primers and the SuperScript III First Strand Synthesis System (Invitrogen-Thermo Fisher Scientific, Waltham, MA). eal-time PCR was performed using SYBR Green and the ABI Prism 7900HT Sequence Detector System (Applied Biosystems-Thermo Fisher Scientific, Waltham, MA). The sequence of primers is listed in Supplemental Table S1. Results were normalized to the internal control β-actin mRNA and the fold change was calculated using the $2^{-\Delta\Delta Ct}$ method of relative quantification (23).

Immunohistochemistry

Immunostaining was performed on formalin-fixed, paraffin-embedded sections that were deparaffinized in xylene and then rehydrated through graded ethanol. Immunohistochemical staining for Ym1, F4/80, and SP-A was performed using the standard avidin-peroxidase technique. Antigen retrieval was carried out with heat using a Decloaking Chamber (Biocare Medical, Concord, CA) for Ym1, proteinase K (Dako, Carpinteria, CA) treatment for 2 min for F4/80, or trypsin (0.1% trypsin in 0.05M Tris-HCl, pH 8.2 and 0.01% $CaCl_2$) treatment for 20 min at 37°C for SP-A. Endogenous peroxidase was blocked using 3% H_2O_2 (15 min) either prior to antigen retrieval (Ym1, F4/80) or after antigen retrieval (SP-A). Non-specific sites were blocked with avidin-biotin blocking reagents for Ym1 and F4/80 immunostaining (Vector Laboratories, Burlingame, CA) or Rodent Block M for SP-A immunostaining (Biocare Medical). Sections were incubated either with goat anti-mouse Ym1 (Chitinase 3-like 3/ECF-L) antibody (AF2446, R&D Systems, Minneapolis, MN) at a dilution of 1:500, followed by biotinylated anti-goat IgG (H+L) secondary antibody (1:2000; Vector Laboratories), rat anti-mouse F4/80 monoclonal antibody (BM8; 123102, BioLegend San Diego, CA) at a dilution of 1:500 followed by biotinylated rabbit anti-rat IgG secondary antibody (1:500; Vector Laboratories), or goat polyclonal SP-A antibody (sc-7699, Santa Cruz Biotechnology, Dallas, TX) at a dilution of 1:100 followed by biotinylated horse anti-goat IgG secondary antibody (1:500; Vector Laboratories). Sections were labeled with the R.T.U. Vectastain Kit (Vector Laboratories) and the antigen-antibody complex was visualized with 3-diaminobenzidine (DAB) chromogen (Dako) followed by hematoxylin counterstaining. Immunohistochemical staining for SP-C was performed using the HRP-polymer technique. Antigen retrieval was performed with Carezyme II: Pepsin (Biocare

Medical) for 3 min at 37°C followed by a 2 min wash in distilled water. Endogenous peroxidase was blocked using 3% H_2O_2 (15 min), and non-specific sites were blocked with Rodent Block M (Biocare Medical). Sections were incubated with rabbit polyclonal anti-Prosurfactant Protein C (AB3786, EMD Millipore, Bellerica, MA) at a dilution of 1:2500, followed by Rabbit on Rodent HRP polymer (Biocare Medical). Sections were treated with DAB and then counterstained with hematoxylin.

Transmission electron microscopy

The tissue samples were collected and fixed in 3% glutaraldehyde. Processing was done with a Leica EM TP processor (Leica Microsystems Inc., North Deerfield, IL). Samples were rinsed with buffer, post-fixed in 2% osmium tetroxide in phosphate buffer, rinsed in distilled water and dehydrated in an ethanol series transitioning into propylene oxide. The samples were then infiltrated with Poly/Bed 812 epoxide resin (Polysciences). After polymerization, selected blocks were trimmed and semithin sections (approximately 0.5 μm thick) were cut, mounted on glass slides, stained with 1% toluidine blue in 1% sodium borate, and examined with a light microscope to ascertain areas of interest. After trimming block faces down to areas of interest, ultrathin sections (70–90 nm thick) were subsequently cut, placed on 100 mesh formvar copper grids and stained with uranyl acetate and lead citrate. Digital images were captured with an Olympus Mega View III side mount camera attached to an FEI Tecnai 120KV transmission electron microscope.

Flow cytometric analysis

Phenotyping of mouse pulmonary immune repertoires was performed using multi-parameter flow cytometry and a panel of antibodies as previously described (24). Briefly, tissues were dissociated into single cell suspensions and stained with a panel of antibodies. Data were acquired using an LSRII flow cytometer (BD Bioscience, San Jose, CA). Data were analyzed using Flowjo X (BD Bioscience). The gating strategy we used is shown in Figure 6A. Absolute numbers of each immune cell type were calculated by multiplying the total cell number recovered from each lung digest by the proportion of a particular cell type as a percentage of live cells.

Bone marrow transplant studies

10 week-old GM-CSFΔARE and WT female mice were used to isolate donor HSC for transplantation. Whole bone marrow was harvested from the tibia, femur, and pelvis of each mouse. For HSC sorting, PE c-Kit antibody (105808, BioLegend, San Diego, CA) and EasySepTM PE Positive Selection Kit II (17684, StemCell Technologies, Cambridge, MA) were used to enrich c-Kit$^+$ cells. Enriched cells were incubated with antibodies against lineage (Ter119,1:200; 116232, BioLegend), B220 (1:200; 103227, BioLegend), CD3 (1:200; 100214, BioLegend), Mac1 (1:200; 101224, BioLegend), Gr1 (1:200; 108434, BioLegend), CD34 (1:50; 11–0341-85, eBioscience-Thermo Fisher Scientific), c-Kit (1:200; 105808, BioLegend), CD150 (1:200; 115914, BioLegend), SCA-1 (1:200; 108126, BioLegend), Flk2 (1:50; 135310, BioLegend), and PI. Then the HSC were sorted as PI$^-$, Lin$^-$, cKit$^+$, Sca1$^+$, CD34$^-$, Flk2$^-$, and CD150$^+$ on a BD FACSAria Fusion flow cytometer (BD Biosciences). In addition, to prepare myeloprotective cells for non-competitive transplantation, whole bone marrow of young B6.SJL-Ptprca Pepcb/BoyJ (B6

CD45.1; stock 002014, The Jackson Laboratory) female mice was incubated with SCA-1 Biotin (108104, BioLegend). Then SCA-1 depleted cells were collected using EasySepTM Biotin Positive Selection Kit II (17683, StemCell Technologies). 150 HSC pooled from donor mice along with 4×10^5 SCA-1 depleted CD45.1 cells per mouse were transplanted into lethally irradiated (9.54 Gy) recipient 8 week-old CD45.1 female mice. Recipients were given TMS water prophylactically for 4 weeks following irradiation. Peripheral blood analysis was performed at 4 week intervals post transplantation.

Peripheral blood analysis for the bone marrow transplant studies

Blood was drawn retro-orbitally. After Ammonium-Chloride-Potassium (ACK) treatment, blood was stained with lineage (Ter119, 1:200; 116228, BioLegend), B220 (1:200; 103224, BioLegend), Mac1 (1:200; 101216, BioLegend), Gr1 (1:200; 108406, BioLegend), CD3 (1:200; 100206, BioLegend), CD45.1 (110714, BioLegend), CD45.2 (109820, BioLegend), and PI and analyzed using a BD FACSCanto II flow cytometer (BD Biosciences). Gating strategy is shown in Supplemental Figure 6.

Whole bone marrow analysis

Bone marrow cells were ACK-treated and then stained with antibodies against lineage (Ter119,1:200; 116204, BioLegend), B220 (1:200; 103204, BioLegend), Mac1 (1:200; 101204, BioLegend), CD3 (1:200; 100244, BioLegend), Gr1 (1:200; 108404, BioLegend), CD34 (1:50; 11–0341-85, eBioscience-Thermo Fisher Scientific), cKit (1:200; 105808, BioLegend), CD150 (1:200; 115914, BioLegend), FcγRα (1:200; 45–0161-82, eBioscience-Thermo Fisher Scientific), Flk2 (1:50; 135310, BioLegend), SCA-1 (1:200; 108126, BioLegend), IL-7Rα (1:100; 135024, BioLegend), CD45.1 (1:100; 61–0453-82, Thermo Fisher Scientific), CD45.2 (1:100; 109847, BioLegend), and PI, then analyzed using a BD FACSymphony A3 (BD Biosciences). Flow cytometry data were analyzed using FlowJo (BD Biosciences) and Cytobank (Beckman Coulter). The gating strategy is shown in Supplemental Figure 7. Biotinylated antibodies were stained using Streptavidin-Pacific Orange (1:200; S32365, Thermo Fisher Scientific), prior to viability staining.

Statistical analysis

Data are presented as means ± SEM. Statistical analysis of growth curves was performed using two-way ANOVA with Sidak's multiple comparison test. Survival curves were analyzed using the Mantel-Cox log-rank test. Scatter plot and ELISA statistical analyses were performed using unpaired Student's t test with Welch's correction. All other statistical analyses were done using an unpaired Student's t test with Holm-Sidak's multiple comparison test. A p-value of < 0.05 was used as the cut-off level for statistical significance. GraphPad Prism 7 (GraphPad Software, Boston, MA) was used for statistical analysis.

Results

Generation and phenotypic analysis of GM-CSFΔARE mice

We generated heterozygous GM-CSFΔARE mice, which express a version of the *Csf2* mRNA that contains a 75 nt deletion of an AU-rich region (ARE; red nucleotides in Figure 1A), using standard homologous recombination techniques. Details are described

in Methods. Schematic representations of the wild-type (WT) allele, the targeting vector, and the targeted alleles before and after crossing to a Flp or Cre recombinase-expressing mouse are shown in Figure 1B. Flp recombinase deletion of the FRT-flanked neomycin selection cassette resulted in the LoxP-flanked exon 4 that contained the WT ARE followed by the ARE-deleted mutant exon 4. Cre recombinase removed the LoxP-flanked exon 4 containing the WT ARE, and ultimately resulted in the ARE-deleted mutant that retained exon 4 (Figure 1B). The use of Meox2-cre, active in early embryos (19), would be expected to result in the expression of the ΔARE *Csf2* mRNA in essentially all tissues.

All heterozygous GM-CSFΔARE mice with Meox2-cre (*Meox2cre*/*Csf2*$^{flARE/+}$, or Het KI) developed respiratory distress and died within a few months after birth. Body weights of control and Het KI mice of both sexes were comparable at two weeks of age, but began to diverge at approximately 3–4 weeks, and Het KI mice weighed significantly less for the rest of their lifespans (Figure 1C). The median survival time for the Het KI mice was approximately 13 weeks (Figure 1C; right panel), and this did not differ between males and females (Figure 1C; left and middle panels). All experiments were therefore conducted in mice of either or both sexes. The following genotypes were considered controls: WT mice with or without Meox2-cre (*Meox2cre*/*Csf2*$^{+/+}$, and *Csf2*$^{+/+}$), and heterozygote mutant mice without Meox2-cre (*Csf2*$^{flARE/+}$). Because of the early onset and relative severity of this phenotype, we did not attempt to characterize homozygous KI mice.

Effect of the GM-CSFΔARE mutation on *Csf2* mRNA stability and protein expression

To determine whether the ARE deletion from the *Csf2* mRNA 3'UTR affected its stability, we measured LPS-induced *Csf2* mRNA levels in bone marrow derived macrophages (BMDM) from control and Het KI mice. *Csf2* mRNA was expressed at very low levels in unstimulated BMDM from control and Het KI mice (Figure 2A, top). This increased to apparent maxima by 1 h in both control and Het KI cells after LPS treatment, at which point the Het KI cells expressed approximately 1.5 times more *Csf2* mRNA than the control cells. *Csf2* mRNA levels returned to baseline at 4 h post-stimulation in control cells, whereas they remained higher than control in the Het KI cells until 6 h post-stimulation (Figure 2A, top). To examine the *Csf2* mRNA stability in this setting, LPS-stimulated BMDM (1h) were treated with Actinomycin D to block transcription, and RNA levels were measured at varying times thereafter (Figure 2B). *Csf2* mRNA levels were consistently higher in the Het KI cells than in control cells, indicating an increase in the stability of *Csf2* mRNA in the Het KI cells. The half-life of *Csf2* mRNA was >120 min in the Het KI cells, whereas the half-life of this transcript in the control cells was approximately 13 min (Figure 2B, top). In the same experiments, we measured the expression and stability of two other well-known LPS-inducible transcripts, *Zfp36* (TTP) and *Tnf* mRNAs. The expression profiles of *Zfp36* and *Tnf* mRNAs after LPS stimulation were similar in the control and Het KI cells (Figure 2A, middle and bottom). In addition, the ΔARE mutation in the Het KI cells did not influence the half-life of these two mRNAs (Figure 2B, middle and bottom).

To determine whether the heterozygous GM-CSFΔARE mutation resulted in increased GM-CSF protein levels, we first measured GM-CSF in serum from either control or Het KI mice. GM-CSF levels were below the assay detection limit in the control animals, but there were

readily detectable levels of GM-CSF protein in the serum from the Het KI mice (Figure 3A). Next, we measured GM-CSF in the bronchoalveolar lavage (BAL) fluid as well as in homogenized lungs after BAL. GM-CSF protein was readily detected in control BAL fluid and the lung homogenate. Levels of GM-CSF at 8–12 weeks of age did not differ between control and Het KI BAL fluids (Figure 3B), but were approximately 2.4-fold greater in the Het KI lung homogenates compared to controls (Figure 3C). The levels of lung *Csf2* mRNA in the 8–12 week-old Het KI mice were 3.8 times higher than those seen in the control mice, and *Csf2* mRNA levels in the Het KI BAL fluid-derived cells were 14 times greater than those seen in control cells (Table 1).

Respiratory phenotype and histopathology of the GM-CSFΔARE mice

Although the Het KI mice appeared normal at birth, they began to show signs of respiratory distress, rapid breathing, weight loss and hunched posture before 2 months of age. Mice were analyzed histologically by 3–4 months of age. The lungs from the Het KI mice appeared enlarged, were white to tan in color, and failed to collapse after removal like lungs from control mice (Figure 4A). We performed complete necropsies with histological analysis on the control and Het KI mice, but the only abnormalities noted were in the lungs of the Het KI mice (Figure 4B). Routine light microscopy on hematoxylin and eosin-stained specimens revealed that large areas of the lungs from the Het KI mice contained dense cellular infiltrates within the alveolar spaces and bronchioles. Higher magnification (right panel of Figure 4C) showed that the infiltrating cells were large epithelioid macrophages admixed with occasional multinucleate giant cells containing fine, acicular eosinophilic crystalline material. The degree of cellular infiltration varied, but generally correlated with the age of the mice and the severity of respiratory distress. In addition to the cellular infiltration, there was multifocal thickening of alveolar walls due to alveolar type II (AT2) cell hyperplasia and fibrosis (Figure 4C).

Microscopic analysis of cells from the Het KI BAL fluid (left panels of Figure 4D) showed enlarged macrophages and some multinucleated giant cells, correlating with the histologic findings. In contrast, there was no significant difference noted between the character of the peritoneal cells collected from control and Het KI mice (right panels of Figure 4D). Cell numbers in the BAL fluid were significantly higher in the Het KI mice compared to the control mice, whereas there was no significant difference in peritoneal cell number (Figure 4E). BAL cells from normal mice were almost all macrophages (99.8 ± 0.25%; mean ± SEM) and few lymphocyte (0.3 ± 0.25%), but the cells from the Het KI BAL fluid contained increased numbers of neutrophils (4.0 ± 2.05%), lymphocytes (2.0 ± 0.9%), and eosinophils (3.8 ± 3.4%) along with macrophages (90.3 ± 6.2%). We also observed increased numbers of white blood cells in the Het KI peripheral blood (Supplemental Figure 1, top). Differential counts showed statistically significant increases in neutrophils, lymphocytes, monocytes, and eosinophils in blood from the Het KI mice (Supplemental Figure 1, bottom).

We also observed turbidity in the BAL fluid from Het KI mice, which led us to examine whether this might reflect an increase in pulmonary surfactant, as is seen in the BAL fluid of GM-CSF KO mice (3, 4). We performed histochemical staining for mucopolysaccharides (PAS staining) and lipids (Oil Red O staining); however, we did not see any evidence of

mucopolysaccharide or lipid accumulation in the lungs from the Het KI mice (Supplemental Figure 2A). BAL fluid was also negative for lipids based on Oil Red O staining of cytospin slides (Supplemental Figure 2B), indicating that the increased turbidity is likely the result of increased cell numbers rather than the accumulation of surfactant in the Het KI lungs.

The histological analysis of the Het KI mice lungs was consistent with a diagnosis of eosinophilic crystalline pneumonia (ECP, acidophilic macrophage pneumonia) (25). We performed immunohistochemical analyses to further characterize this phenotype. First, we analyzed the identity of the cellular infiltrates using anti-F4/80 antibody, a well-established macrophage marker. A few F4/80 positive cells were seen in the control lungs (upper left panel of Figure 5A), whereas all cellular infiltrates in the Het KI lungs showed strong cytoplasmic immunoreactivity to F4/80 (upper right panel of Figure 5A). Next, we examined whether the cellular infiltrates expressed Ym1 (Chil3, chitinase-like 3), a well-established marker for eosinophilic crystalline pneumonia (26). As shown in the lower right panel of Figure 5A, most if not all of the infiltrating cells in the Het KI lungs expressed Ym1, similar to the results seen with F4/80 staining. Ultrastructural analysis of the lungs using transmission electron microscopy demonstrated the presence of electron-dense, angular to rectangular, needle-shaped crystalloid inclusions within the cytoplasm of the infiltrating macrophages in the Het KI lungs (Figure 5B), as previously seen in this type of pneumonia (27, 28).

Surfactant protein expression in GM-CSFΔARE mice

Because GM-CSF plays an essential role in maintaining surfactant homeostasis in the lung, we examined the expression of two surfactant-associated proteins (SP-A and SP-C) in control and Het KI lungs. Expression of SP-A and SP-C were observed in the epithelial cells of alveoli and bronchioles in control lungs (left panels, Figure 5C). Notable immunostaining of SP-A but not SP-C was seen in the cellular infiltrates in the Het KI lungs (right panels, Figure 5C). We also observed relatively high levels of SP-C in the Het KI alveolar epithelial cells, perhaps reflecting the AT2 cell hyperplasia observed in the Het KI lung. We measured mRNA levels encoding SP-A (*Sftpa1*) and SP-C (*Sftpc*) in the lung and the cells from BAL fluid. The levels of *Sftpa1* and *Sftpc* mRNAs in the Het KI lungs were 2.5-times and 7.2-times lower than in control mice, respectively (Table 1), suggesting that the accumulation of SP-A in the cellular infiltrate may be the result of defects in surfactant protein catabolism in the alveolar macrophage (AM) and not the result of increased protein production. However, this remains to be proved.

Phenotypic analysis of alveolar macrophages in GM-CSFΔARE mice

We next performed phenotypic analyses of lung and BAL macrophages in control and Het KI mice using flow cytometry (Figure 6A). In control animals, we observed typical AM (SiglecF^{+}CD11b^{-}CD88^{+}) in BAL fluid and lung as well as pulmonary interstitial macrophages (IM; SiglecF^{-}CD11b^{+}CD88^{+}) in the lung (Figures 6B, 6C and Supplemental Table S2). In the control mice, BAL fluid contained 98.5% AM and 1.4% IM; lung contained 84.2% AM and 14.7% IM. In the Het KI mice, we observed the accumulation of AM-like cells in BAL fluid (R4, 96.1% in CD11b vs. SiglecF plot) and lungs (R6, 81.3% in CD11b vs. SiglecF plot). These AM-like cells expressed intermediate levels of CD11b,

a finding that was different from normal AM, which were CD11b negative (Figure 6B). In addition, normal AM were characterized by high levels of CD88, whereas the expression of CD88 was negative or low in the AM-like cells in the Het KI mice (Figure 6C). Specifically, about 95% of AM (AMØs) expressed CD88 in control BAL fluid and lungs, whereas only 21% of R4 cells and 5.5% of R6 cells expressed CD88 in Het KI BAL fluid and lungs, respectively (Figure 6D). Based on the expression patterns of CD11b and CD88, AM and AM-like cells (R6) from the Het KI lungs occupied distinctive spatial locations on the flow plot (left panel in Figure 6E). IM in control mice (15.3% in CD11b vs. SiglecF plot) and IM-like cells (R7, 16.8% in CD11b vs. SiglecF plot) in Het KI mice showed similar expression patterns of SiglecF, CD11b, and CD88. However, IM-like cells contained a subpopulation of high CD11c-expressing cells (right panel in Figure 6E). In addition, abnormal accumulation of $SiglecF^{-}CD11b^{+}$ cells (R5, 3.8% in CD11b vs. SiglecF plot) was observed in the Het KI BAL fluid. $SiglecF^{-}CD11b^{+}$ cells have been described as infiltrating alveolar spaces under inflammatory conditions (29, 30). A summary of the immune cell populations in lung and BAL fluid is shown in Supplemental Table S3.

Pulmonary microenvironment in GM-CSFΔARE mice

Previous reports examining the pulmonary microenvironment of GM-CSF KO mice showed an elevation of both M1 (classical macrophage activation, Th1) and M2 (alternative activation, Th2) phenotypic markers (7). We analyzed the level of cytokines and chemokines (M-CSF, IL-6, IFNγ, MIP1α/CCL3, MIP1β/CCL4, KC/CXCL1, IP-10/CXCL10, Rantes/CCL5, IL-17) related to phenotypic markers for M1 and M2 in the BAL fluid by ELISA (Table 2). We observed elevations in the levels of all these cytokines and chemokines in the Het KI BAL fluid. Of note, increased levels of M-CSF, IL-6, IFNγ, and Rantes/CCL5 in GM-CSF KO mice have been reported (7, 31, 32). The result suggests that the overproduction of GM-CSF in the Het KI mice also resulted in an elevation of both M1 and M2 phenotypic markers. In addition, increased chemokines (MIP1α/CCL3, MIP1β/CCL4, KC/CXCL1, IP-10/CXCL10) in Het KI BAL fluid might be related to the accumulation of macrophages in the lung.

Altered lung gene expression in GM-CSFΔARE mice

We also analyzed the expression levels of several genes that have been shown to play a regulatory role in surfactant homeostasis (*Abca3*, *Cd36*, *Cyp27a1*, *Fabp1*, *Adgrf5*/Gpr116, *Sftpa1*, *Sftpc*, *Nr1h3*, and *Nr1h2*), and AM differentiation (*Pparg*, *Spi1*/PU.1, *Itgam*/CD11b, *Itgax*/CD11c, and *Siglecf*) in lung and BAL fluid-derived AM. Results are shown as the ratio between control and Het KI average values (Table 1). In general, the genes expressed in the epithelium were down-regulated (*Cd36*, *Cyp27a1*, *Adgrf5*, *Sftpa1*, and *Sftpc*), whereas the genes expressed in the AM were up-regulated (*Abca3*, *Nr1h3*, *Nr1h2*, *Itgam*, and *Itgax*). Expression profiles of *Itgam* (CD11b), *Itgax* (CD11c), and *Siglecf* were consistent with the flow cytometry profiles. It has been reported that *Pparg* expression is up-regulated by GM-CSF (33); however, in the present experiments, its expression in the Het KI AM was not up-regulated. Expression of *Nr1h3* and *Nr1h2*, transcription factors controlling cholesterol metabolism-related factors in macrophages (34), was 7.6 times and 3.6 times increased, respectively, in the Het KI AM. Expression of *Adgrf5*, which has been shown to be an essential factor for surfactant metabolism (35), was 13.9-fold decreased in Het KI lung.

Overall, it seems likely that the attenuation of surfactant production from the epithelium and the activation of lipid metabolism in the AM reflect the Het KI lung phenotype.

Transplantation of GM-CSFΔARE hematopoietic stem cells into WT mice

To investigate the possible effect of overproduction of GM-CSF in the hematopoietic system on the development of the characteristic eosinophilic crystalline pneumonia, we performed non-competitive transplantations of hematopoietic stem cells (HSC) from young Het KI mice into irradiated WT recipients as described in Methods. We monitored the body weights and general appearance of the transplanted mice for up to 28 weeks, and analyzed peripheral blood cells every 4 weeks to determine chimerism levels. Sixteen weeks after the transplant, there was no significant difference in the donor chimerism of recipient mice who received HSC from either the Het KI mice or control mice (approximately 80%) (Supplemental Figure 3A, top). The extent of chimerism was similar between the two groups of recipients evaluated at 20 and 28 weeks (Supplemental Figure 3A, bottom). None of the mice transplanted with Het KI HSC exhibited any evidence of weight loss or respiratory distress during the full duration of the study, which extended to 28 weeks after transplantation. In addition, histopathological evaluation of the lungs at 20 and 28 weeks after transplantation by a pathologist blinded to the genotypes found no apparent differences on average between the lungs from mice transplanted with cells from Het KI and WT mice (Supplemental Figure 4).

The relative proportions of various donor derived peripheral blood cells were similar between the mice transplanted with Het KI or WT HSC at 20 weeks post-transplant and were maintained through 28 weeks (Supplemental Figure 3B and 3C). The frequencies of the donor-derived bone marrow cells were analyzed in three subsets (myeloid progenitor cells, early progenitor cells (LSK) and HSC subsets). The proportion of $CD150^{Hi}$ myeloid-biased cells in the HSC subset and frequency of megakaryocyte erythrocyte progenitors (MEP) in the myeloid progenitor subset were higher in the Het KI HSC transplanted mice at 20 weeks, but those differences were not seen at 28 weeks after transplantation (Supplemental Figure 5). These results demonstrate that the disruption of *Csf2* mRNA turnover regulation in HSC and cells derived from them did not interfere with complete and apparently normal bone marrow reconstitution during this study. It also suggests that the effect of ARE deletion within the *Csf2* mRNA in the cells derived from the hematopoietic system was not likely to be the cause of the abnormal macrophage accumulation in the alveolar spaces in the Het KI mice.

Mice with a GM-CSF ARE deletion in pulmonary alveolar epithelial cells

The bone marrow transplant studies suggested that the ARE deletion within the *Csf2* mRNA in cells derived from hematopoietic precursors is unlikely to mediate the severe eosinophilic crystalline pneumonia phenotype seen in the Het KI mice. Several previous studies have identified pulmonary epithelial cells, specifically AT2 cells, as possible sources of GM-CSF in normal AM function and surfactant homeostasis (36–38). To test whether possible overproduction of GM-CSF from AT2 cells could be a driving force for the Het KI lung phenotype, we generated an AT2 cell-specific GM-CSFΔARE mouse line. For this purpose, $Csf2^{flARE/flARE}$ mice were crossed with tamoxifen-inducible AT2 cell-specific cre

expression mice (Sftpc-creER^{T2}) (20). Without tamoxifen treatment, most *Csf2*$^{flARE/flARE}$ mice with Sftpc-creER^{T2} (either homozygous or heterozygous for cre allele) did not exhibit any deleterious effects such as weight loss or dyspnea for more than a year. However, 13.5% (25 out of 185 mice) of *Csf2*$^{flARE/flARE}$ with Sftpc-creER^{T2} mice exhibited apparent respiratory distress or were found dead. In contrast, only 2.6% (5 out of 191 mice) of *Csf2*$^{flARE/flARE}$ without Sftpc-creER^{T2} mice were found dead during the same period. This is likely to be due to some spontaneous cre expression in the absence of tamoxifen. The original report describing the Sftpc-creER^{T2} mice demonstrated that about 25% of mice had exhibited spontaneous cre expression without tamoxifen treatment (20). We then treated 4 month-old *Csf2*$^{flARE/flARE}$ or *Csf2*$^{flARE/+}$ mice, with or without Sftpc-creER^{T2}, with tamoxifen, and monitored body weights and other signs for 19 weeks. When mice began exhibiting significant body weight loss and respiratory distress, lung tissue was collected and analyzed histologically. As shown in Figure 7A, mice homozygous for *Csf2*$^{flARE/flARE}$ with Sftpc-creER^{T2} (homozygous or heterozygous for cre allele) grew normally for varying lengths of time after tamoxifen treatment. However, these mice eventually began losing weight and displayed apparent respiratory distress about 13 weeks after tamoxifen treatment. The *Csf2*$^{flARE/flARE}$ mice with homozygous Sftpc-creER^{T2} appeared to develop the deleterious phenotype faster than the mice with heterozygous Sftpc-creER^{T2} (middle and bottom panels in Figure 7A). Mice that were heterozygous for *Csf2*$^{flARE/+}$ with homozygous Sftpc-creER^{T2} did not show significant body weight loss until 19 weeks after tamoxifen treatment (top panel in Figure 7A). However, the mice developed respiratory distress at that time. The tamoxifen-treated cre negative *Csf2*$^{flARE/flARE}$ mice did not lose weight and did not show any signs of respiratory distress throughout the course of the experiment (open circle and square in Figure 7A). We did not observe any obvious sex differences in genotype-dependent phenotypes. Histopathological results of both homozygous *Csf2*$^{flARE/flARE}$ and heterozygous *Csf2*$^{flARE/+}$ mice possessing Sftpc-creER^{T2} exhibited essentially identical lung histopathological phenotypes to those from the original Het KI mice (Figure 7B and 7C), i.e., dense infiltration and consolidation with alveolar macrophages.

Next, we generated a myeloid cell-specific GM-CSFΔARE mouse line. *Csf2*$^{flARE/flARE}$ mice were crossed with myeloid-specific cre expression mice (LysM-cre) (21). *Csf2*$^{flARE/flARE}$ mice with heterozygous LysM-cre developed respiratory distress and died at approximately 9 months of age. Histopathological results from 8 month-old mouse lungs of this genotype looked essentially identical to the original 10 week-old Het KI lungs (top panel in Figure 7D compared to Figure 4B). At 4 months of age, macrophages could be found accumulating in a portion of the lung lobes (bottom panel in Figure 7D). However, the accumulation of AM occurred much later in the myeloid-specific GM-CSFΔARE mice than in the other mouse lines (Het KI and AT2 cell-specific GM-CSFΔARE).

These data suggest that AT2 cell-mediated GM-CSF overproduction caused by the GM-CSF mRNA stabilization mimicked the phenotype seen in the Het KI mice, and is thus likely to be responsible for mediating most of the abnormal AM accumulation in the Het KI lungs. Myeloid cell-mediated GM-CSF overproduction could also be involved in some of the AM accumulation, but it occurred so much later in life that it is unlikely to be the immediate cause of the abnormal AM accumulation seen in the Het KI lungs.

Discussion

The most important finding of this study is that mice with a single mutant allele of *Csf2,* expressing a stabilized form of the *Csf2* mRNA, develop a single, specific, localized and lethal lesion, i.e., dense packing of the lungs with AM followed by respiratory failure at a relatively young age. We did not find abnormalities of macrophage accumulation elsewhere in the body. Also, hematopoiesis was almost unaffected in the mutant mice or in the wild-type mice transplanted with mutant HSC. The finding that the increased stability of approximately half of expressed *Csf2* transcripts in all the cells of the mouse leads to this single abnormality suggests a critical role for GM-CSF expression in regulating alveolar macrophage accumulation and perhaps function, a finding supported by the cell-specific expression of the mutation in AT2 cells. An important caveat of this study is that we did not attempt to make homozygous mice because of the early onset and severity of the lesion seen in the heterozygotes. However, it seems possible that even greater overproduction of GM-CSF throughout the body might reveal other physiological processes in which the regulated stability of this cytokine transcript plays an important function.

Although the role of AU-rich regions in the 3'UTR of the *CSF2* mRNA in controlling the stability of that mRNA has been known for more than 30 years (15), their contribution to the physiology of GM-CSF in the intact organism has not been elucidated. There have been several previous reports of models involving the overexpression of GM-CSF *in vivo* (2, 39, 40). In one case, transgenic mice were developed in which a retroviral promoter drove the expression of mouse *Csf2* genomic DNA. This form of general GM-CSF overproduction led to the infiltration of macrophages in the peritoneal cavity, muscle, and eyes (2), resulting in blindness, muscle wasting and death at 2–4 months of age, that was to some extent sex-dependent (2). Another mouse model used the potent and universal CMV promoter to drive the expression of mouse *Csf2* genomic DNA, with or without the 3'-UTR ARE. Regardless of ARE status, these mice were not viable after birth. CMV promoter-mediated universal overexpression of GM-CSF may have contributed to the early death seen in both types of transgenic mice. However, these authors found detectable expression of transgene-derived *Csf2* mRNA in the ARE-deleted embryos but not in the ARE-retaining or non-transgenic embryos, implying that a change in stability could have led to this difference (41).

The effect of lung-specific GM-CSF overexpression has been described using SP-C-GM transgenic mice (36, 37). These mice carried the human SP-C promoter fused to a mouse *Csf2* cDNA transgene, so that GM-CSF was overexpressed in lung AT2 cells. This transgene was shown to correct the defective lung phenotype of GM-CSF KO mice, providing further evidence that AT2 cell-derived GM-CSF regulates surfactant homeostasis (36, 37). Increased GM-CSF level in the BAL fluid collected from the SP-C-GM transgenic mice was seen, along with increased numbers of AM. However, these transgenic mice did not exhibit any significant health issues, with the exception of one founder that failed to breed and became moribund at 4 months of age. The failed founder mouse exhibited pulmonary infiltration of AM that somewhat resembled the phenotype described here (36, 37). More recently, a report showed that SP-C-GM transgenic mice exhibited marked accumulations of AM as well as increased giant cell number and alveolar cell hyperplasia by 10 months of age, leading to overall increased mortality (median survival of 10.5 months) (42). The

presence of intracellular crystals was not described in that report. The mice also exhibited polycythemia, so that average hematocrits at 9 months were 65 % in the transgenic mice vs. 42 % in the control mice, along with six-fold increases in blood levels of erythropoietin (42). This may be due to chronic lung disease-induced hypoxemia in the SP-C-GM transgenic mice. Overall, these results support the idea that AT2 cell-derived GM-CSF causes AM accumulation in the lung. However, it seems likely that the GM-CSF expression in the SP-C-GM transgenic mice differed in both amount and regulation from that endogenous GM-CSF expression.

The present model differs from previous models in that the expression of GM-CSF is controlled by the endogenous *Csf2* gene promoter, which is an advantage in analyzing the normal physiological roles of GM-CSF and the contribution of post-transcriptional mRNA turnover regulation in the GM-CSF expression regulation. In addition, the GM-CSF overproduction caused by the enhancement of mRNA stability can be controlled in a tissue-selective manner by crossing with tissue/cell type specific cre-expressing mouse lines, as we demonstrated in the lung AT2 cell-specific GM-CSFΔARE mice and myeloid-cell-specific GM-CSFΔARE mice. These features are distinct from previous GM-CSF overproducing mouse models.

The RNA binding protein tristetraprolin (TTP) can bind to ARE elements in mRNAs and enhance their decay (43). We demonstrated previously that the *Csf2* mRNA was a direct target of TTP in bone marrow-derived stromal cells (BMSC) (44). Although the overall phenotype of TTP KO mice is complex, one major aspect is profound myeloid hyperplasia (45). Although many aspects of the TTP-deficiency phenotype could be largely rescued by interbreeding with TNF receptor 1 deficient mice, the myeloid hyperplasia seen in bone marrow was not rescued by this intervention (46). This led to the hypothesis that increased levels of circulating GM-CSF, as a result of the stabilized *Csf2* mRNA in the GM-CSFΔARE mice, might recapitulate the myeloid hyperplasia phenotype seen in the TTP KO mice. We did observe slightly increased white blood cell numbers, especially neutrophils, in the peripheral blood from the GM-CSFΔARE mice. However, we did not find notable myeloid hyperplasia in the GM-CSFΔARE bone marrow, and the profound macrophage infiltration in the lung that is seen in the GM-CSFΔARE mice has never been observed in TTP KO mice. Thus, although TTP is undoubtedly responsible for some aspects of *Csf2* mRNA regulation, these effects are not profound enough to lead to the lung phenotypes described here. Similarly, we cannot ascribe the myeloid hyperplasia characteristic of the TTP KO mice to *Csf2* mRNA stabilization.

The lung phenotype exhibited by the GM-CSFΔARE mice can be described as eosinophilic crystalline pneumonia, sometimes found sporadically as a spontaneous background lesion in aging mice of certain strains, and occasionally a cause of respiratory distress and death (25). It has also been seen in certain genetically modified mice (e.g., NADPH oxidase subunit $p47^{phox}$ KO) (47) and in mice with concurrent pulmonary neoplasms or infectious diseases (26, 48–51), as well as in certain models of allergic pulmonary disease (52). AM from mice with this condition contain characteristic crystals composed mainly of Ym1 protein, a lectin of unknown function secreted by macrophages (53), that may play a role in host immune defense, allergic/inflammatory responses, and eosinophil chemotaxis (49, 54, 55).

Although p47^{phox} or neutrophil cytosolic factor 1 (*Ncf1*)-deficient mice exhibit a similar lung phenotype to that described here (47), we found no changes in *Ncf1* mRNA levels in lungs from the GM-CSFΔARE mice (data not shown), arguing against its involvement in the current phenotype.

The pulmonary phenotype of GM-CSFΔARE mice is also similar to a human disease, "desquamative interstitial pneumonia (DIP)". DIP is an uncommon condition often associated with smoking in which there are abnormal accumulations of AM along with some eosinophils (56, 57). The overproduction of GM-CSF from alveolar cells could be involved in the pathogenesis of human DIP (42). However, intracellular crystals have not been described in AM from patients with DIP.

It was an unexpected observation that the *Pparg* mRNA levels were not up-regulated in the AM collected from BAL fluid in the GM-CSFΔARE mice. Previous reports suggested that GM-CSF can increase the expression of PPARγ in AM. For instance, *Pparg* mRNA levels were essentially undetectable in AM from GM-CSF KO mice and PAP patients (33, 58), whereas GM-CSF therapy normalized the *Pparg* mRNA expression levels in AM of PAP patients (33). The lower *Pparg* mRNA expression levels in the AM from GM-CSFΔARE mice suggest that the accumulated AM might not be fully functional, perhaps correlating with their phenotypic abnormalities observed by flow cytometry.

The source of AM is somewhat controversial, but is thought to involve fetal monocytes with minimal contribution from circulating monocytes in the adult. Fetal monocytes (Ly6C^{hi}CD11b^{hi}) colonize the lung at approximately embryonic day 12.5 (E12.5), then begin to differentiate on about E18.5, with mature AM (SiglecF^{hi}CD11c^{hi}) appearing between postnatal days 1 and 3 (59). The importance of GM-CSF expression during this period to the eventual appearance of mature AM was illustrated by an experiment in GM-CSF KO mice (59). Specifically, treatment of the KO neonates with GM-CSF during the first days of life was able to rescue the AM and allow them to self-maintain for several weeks, although it could not prevent the development of PAP in the KO mice (59). More recently, a study using AT2 cell-specific GM-CSF KO mice showed that PAP developed in the adult mice, along with decreased numbers of AM. This was in contrast to the findings in hematopoietic cell-specific GM-CSF KO mice, which did not exhibit PAP (38). These results are consistent with our observations that AT2 cell-specific GM-CSFΔARE mice developed increased AM and full-blown, lethal pneumonia, but that this was not seen in the mice transplanted with bone marrow from the GM-CSFΔARE mice. It is possible that the AT2 cell-derived GM-CSF enhanced the proliferation of AM instead of, or in addition to, the infiltration of macrophages into the alveolar spaces. In support of this idea, a previous study has demonstrated that the resident AM pool is maintained by the local proliferation of resident AM rather than by the recruitment of circulating precursor cells during the early stages of allergic inflammation (60). This mechanism may play a role in the phenotype of the GM-CSFΔARE mice.

Taken together, these observations suggest that AT2 cell-expressed GM-CSF is essential for maintaining the AM population and function for surfactant homeostasis in the adult lung, and our data suggest that *Csf2* mRNA turnover is essential for this regulation. These results

also suggest that the GM-CSF level is tightly regulated for the AM activity. It also implies that the effective dose range of GM-CSF for PAP patients may be very narrow, possibly providing a partial explanation for the relative lack of success of GM-CSF therapies in PAP patients (9, 61, 62).

GM-CSF is known to be a potent factor for granulocyte and monocyte differentiation (63). However, we observed almost no impact on bone marrow cell populations or the peripheral blood cell profile in the mice transplanted with HSC from GM-CSFΔARE mice. This result suggests that increasing *Csf2* mRNA stability does not significantly affect the differentiation of bone marrow monocytes or macrophages under normal physiological conditions. Future studies will be needed to evaluate the significance of *Csf2* mRNA turnover regulation in hematopoietic cell differentiation under various stressful conditions, such as inflammatory diseases. Interestingly, our mice did not exhibit increases in hematocrit, as reported recently for the SP-C-GM transgenic mice (42). However, their mice were evaluated at 9 months of age, whereas our mice were evaluated at about 12 weeks of age. Endogenous promoter-driven GM-CSF in the GM-CSFΔARE mice caused them to develop pulmonary distress and death much earlier than the SP-C-GM transgenic mice, probably too early to observe the effects of chronic hypoxemia.

Previous studies have focused on the *Csf2* gene promoter as the primary regulator of GM-CSF expression in response to physiological signals (64, 65). However, we demonstrate here that *Csf2* mRNA turnover in normal physiological conditions is essential to the regulation of AM homeostasis but, at least in this heterozygous model, not hematopoietic cell differentiation. This very specific phenotype in mice in which essentially every cell expresses stabilized *Csf2* mRNA is somewhat surprising. Even more so was the replication of the phenotype by stabilizing *Csf2* mRNA in one specific cell type, the AT2 cells. In contrast, the stabilization of *Csf2* mRNA in macrophages and other myeloid cells replicated certain aspects of the lung phenotype only much later in life (9 months versus 13 weeks in the AT2 cells). The new mouse model described here should allow us to unravel the relative importance of transcriptional and post-transcriptional regulation in overall GM-CSF expression in the lung.

Supplementary Material

Refer to Web version on PubMed Central for supplementary material.

Acknowledgments

Supported in part by the Intramural Research Program of the NIH (NIEHS and NIA). Also supported by NIH grants K08HL121185 and R01ES027574 to Y-RY and RMT, respectively. We thank Dee Wenzel and the NIEHS Comparative Medicine Branch staff for animal care; the NIEHS Comparative & Molecular Pathogenesis Branch, Pathology Support Group, for histology; and the Clinical Pathology Group for running the CBC. We greatly appreciate the comments of Drs. Michael Fessler and Donald Cook on the manuscript.

Data Availability Statement

The data that support the findings of this study are available on request to the corresponding author.

Nonstandard abbreviations

GM-CSF	Granulocyte-macrophage colony-stimulating factor
ARE	adenine-uridine rich element
KO	knock-out
PAP	pulmonary alveolar proteinosis
AM	alveolar macrophages
TNF	tumor necrosis factor α
UTR	untranslated region
KI	knock-in
WT	wild-type
BMDM	bone marrow derived macrophages
BAL	bronchoalveolar lavage
AT2	alveolar type II
TTP	tristetraprolin
DIP	desquamative interstitial pneumonia

References

Uncategorized References

1. Clark SC, and Kamen R. The human hematopoietic colony-stimulating factors. Science. 1987;236(4806):1229–37. [PubMed: 3296190]
2. Lang RA, Metcalf D, Cuthbertson RA, Lyons I, Stanley E, Kelso A, et al. Transgenic mice expressing a hemopoietic growth factor gene (GM-CSF) develop accumulations of macrophages, blindness, and a fatal syndrome of tissue damage. Cell. 1987;51(4):675–86. [PubMed: 3499986]
3. Dranoff G, Crawford AD, Sadelain M, Ream B, Rashid A, Bronson RT, et al. Involvement of granulocyte-macrophage colony-stimulating factor in pulmonary homeostasis. Science. 1994;264(5159):713–6. [PubMed: 8171324]
4. Stanley E, Lieschke GJ, Grail D, Metcalf D, Hodgson G, Gall JAM, et al. Granulocyte/Macrophage Colony-Stimulating Factor-Deficient Mice Show No Major Perturbation of Hematopoiesis but Develop a Characteristic Pulmonary Pathology. Proceedings of the National Academy of Sciences of the United States of America. 1994;91(12):5592–6. [PubMed: 8202532]
5. Berclaz P-Y, Shibata Y, Whitsett JA, and Trapnell BC. GM-CSF, via PU.1, regulates alveolar macrophage FcγR-mediated phagocytosis and the IL-18/IFN-γ–mediated molecular connection between innate and adaptive immunity in the lung. Blood. 2002;100(12):4193–200. [PubMed: 12393686]
6. Ditiatkovski M, Toh B-H, and Bobik A. GM-CSF Deficiency Reduces Macrophage PPAR-γ Expression and Aggravates Atherosclerosis in ApoE-Deficient Mice. Arteriosclerosis, Thrombosis, and Vascular Biology. 2006;26(10):2337–44. [PubMed: 16873730]
7. Dalrymple H, Barna BP, Malur A, Malur AG, Kavuru MS, and Thomassen MJ. Alveolar macrophages of GM-CSF knockout mice exhibit mixed M1 and M2 phenotypes. BMC Immunol. 2013;14:41. [PubMed: 24044676]

8. Trapnell BC, and Whitsett JA. Gm-CSF regulates pulmonary surfactant homeostasis and alveolar macrophage-mediated innate host defense. Annu Rev Physiol. 2002;64:775–802. [PubMed: 11826288]
9. Trapnell BC, Nakata K, Bonella F, Campo I, Griese M, Hamilton J, et al. Pulmonary alveolar proteinosis. Nat Rev Dis Primers. 2019;5(1):16. [PubMed: 30846703]
10. Tazawa R, Ueda T, Abe M, Tatsumi K, Eda R, Kondoh S, et al. Inhaled GM-CSF for Pulmonary Alveolar Proteinosis. N Engl J Med. 2019;381(10):923–32. [PubMed: 31483963]
11. Mir-Kasimov M, Sturrock A, McManus M, and Paine R, 3rd. Effect of alveolar epithelial cell plasticity on the regulation of GM-CSF expression. Am J Physiol Lung Cell Mol Physiol. 2012;302(6):L504–11. [PubMed: 22227205]
12. Koeffler HP, Gasson J, and Tobler A. Transcriptional and posttranscriptional modulation of myeloid colony-stimulating factor expression by tumor necrosis factor and other agents. Mol Cell Biol. 1988;8(8):3432–8. [PubMed: 2463477]
13. Osborne CS, Vadas MA, and Cockerill PN. Transcriptional regulation of mouse granulocyte-macrophage colony-stimulating factor/IL-3 locus. J Immunol. 1995;155(1):226–35. [PubMed: 7602099]
14. Cockerill PN, Osborne CS, Bert AG, and Grotto RJ. Regulation of GM-CSF gene transcription by core-binding factor. Cell Growth Differ. 1996;7(7):917–22. [PubMed: 8809409]
15. Shaw G, and Kamen R. A Conserved AU Sequence from the 3 ‘ Untranslated Region of GM-CSF mRNA Mediates Selective mRNA Degradation. Cell. 1986;46:659–67. [PubMed: 3488815]
16. Buzby JS, Brewer G, and Nugent DJ. Developmental regulation of RNA transcript destabilization by A + U-rich elements is AUF1-dependent. J Biol Chem. 1999;274(48):33973–8. [PubMed: 10567360]
17. Chen C-YA, and Shyu A-B. AU-rich elements: characterization and importance in mRNA degradation. Trends in Biochemical Sciences. 1995;20(11):465–70. [PubMed: 8578590]
18. Barreau C, Paillard L, and Osborne HB. AU-rich elements and associated factors: are there unifying principles? Nucleic Acids Res. 2005;33(22):7138–50. [PubMed: 16391004]
19. Tallquist MD, and Soriano P. Epiblast-Restricted Cre Expression in MORE Mice: A Tool to Distinguish Embryonic vs. Extra-Embryonic Gene Function. Genesis. 2000;26(2):113–5. [PubMed: 10686601]
20. Rock JR, Barkauskas CE, Cronce MJ, Xue Y, Harris JR, Liang J, et al. Multiple stromal populations contribute to pulmonary fibrosis without evidence for epithelial to mesenchymal transition. Proc Natl Acad Sci U S A. 2011;108(52):E1475–83. [PubMed: 22123957]
21. Clausen BE, Burkhardt C, Reith W, Renkawitz R, and Forster I. Conditional gene targeting in macrophages and granulocytes using LysMcre mice. Transgenic Res. 1999;8(4):265–77. [PubMed: 10621974]
22. Carballo E, Gilkeson GS, and Blackshear PJ. Bone marrow transplantation reproduces the tristetraprolin-deficiency syndrome in recombination activating gene-2 (−/−) mice. Evidence that monocyte/macrophage progenitors may be responsible for TNFalpha overproduction. J Clin Invest. 1997;100(5):986–95. [PubMed: 9276715]
23. Livak KJ, and Schmittgen TD. Analysis of relative gene expression data using real-time quantitative PCR and the 2(−Delta Delta C(T)) Method. Methods. 2001;25(4):402–8. [PubMed: 11846609]
24. Yu YR, O’Koren EG, Hotten DF, Kan MJ, Kopin D, Nelson ER, et al. A Protocol for the Comprehensive Flow Cytometric Analysis of Immune Cells in Normal and Inflamed Murine Non-Lymphoid Tissues. PLoS One. 2016;11(3):e0150606. [PubMed: 26938654]
25. Hoenerhoff MJ, Starost MF, and Ward JM. Eosinophilic crystalline pneumonia as a major cause of death in 129S4/SvJae mice. Veterinary Pathology. 2006;43(5):682–8. [PubMed: 16966445]
26. Marchesi F, Monestiroli SV, Capillo M, Gobbi A, Minucci S, Pelicci PG, et al. Eosinophilic crystals as a distinctive morphologic feature of a hyaline droplet nephropathy in a mouse model of acute myelogenous leukaemia. J Vet Med A Physiol Pathol Clin Med. 2003;50(2):103–7. [PubMed: 12667201]
27. Pantanowitz L, and Balogh K. Charcot-Leyden crystals: pathology and diagnostic utility. Ear Nose Throat J. 2004;83(7):489–90. [PubMed: 15372922]

28. Carson HJ, Buschmann RJ, Weisz-Carrington P, and Choi YS. Identification of Charcot-Leyden crystals by electron microscopy. Ultrastruct Pathol. 1992;16(4):403–11. [PubMed: 1502737]
29. Duan M, Steinfort DP, Smallwood D, Hew M, Chen W, Ernst M, et al. CD11b immunophenotyping identifies inflammatory profiles in the mouse and human lungs. Mucosal Immunol. 2016;9(2):550–63. [PubMed: 26422753]
30. Kirby AC, Raynes JG, and Kaye PM. CD11b regulates recruitment of alveolar macrophages but not pulmonary dendritic cells after pneumococcal challenge. J Infect Dis. 2006;193(2):205–13. [PubMed: 16362884]
31. Shibata Y, Berclaz PY, Chroneos ZC, Yoshida M, Whitsett JA, and Trapnell BC. GM-CSF regulates alveolar macrophage differentiation and innate immunity in the lung through PU.1. Immunity. 2001;15(4):557–67. [PubMed: 11672538]
32. Su YC, Rolph MS, Hansbro NG, Mackay CR, and Sewell WA. Granulocyte-macrophage colony-stimulating factor is required for bronchial eosinophilia in a murine model of allergic airway inflammation. J Immunol. 2008;180(4):2600–7. [PubMed: 18250471]
33. Bonfield TL, Farver CF, Barna BP, Malur A, Abraham S, Raychaudhuri B, et al. Peroxisome proliferator-activated receptor-gamma is deficient in alveolar macrophages from patients with alveolar proteinosis. Am J Respir Cell Mol Biol. 2003;29(6):677–82. [PubMed: 12805087]
34. Repa JJ, and Mangelsdorf DJ. The role of orphan nuclear receptors in the regulation of cholesterol homeostasis. Annu Rev Cell Dev Biol. 2000;16:459–81. [PubMed: 11031244]
35. Yang MY, Hilton MB, Seaman S, Haines DC, Nagashima K, Burks CM, et al. Essential regulation of lung surfactant homeostasis by the orphan G protein-coupled receptor GPR116. Cell Rep. 2013;3(5):1457–64. [PubMed: 23684610]
36. Huffman JA, Hull WM, Dranoff G, Mulligan RC, and Whitsett JA. Pulmonary epithelial cell expression of GM-CSF corrects the alveolar proteinosis in GM-CSF-deficient mice. J Clin Invest. 1996;97(3):649–55. [PubMed: 8609219]
37. Huffman Reed JA, Rice WR, Zsengeller ZK, Wert SE, Dranoff G, and Whitsett JA. GM-CSF enhances lung growth and causes alveolar type II epithelial cell hyperplasia in transgenic mice. Am J Physiol. 1997;273(4):L715–25. [PubMed: 9357845]
38. Gschwend J, Sherman SPM, Ridder F, Feng X, Liang HE, Locksley RM, et al. Alveolar macrophages rely on GM-CSF from alveolar epithelial type 2 cells before and after birth. J Exp Med. 2021;218(10).
39. Johnson GR, Gonda TJ, Metcalf D, Hariharan IK, and Cory S. A lethal myeloproliferative syndrome in mice transplanted with bone marrow cells infected with a retrovirus expressing granulocyte-macrophage colony stimulating factor. EMBO J. 1989;8(2):441–8. [PubMed: 2542015]
40. Xing Z, Braciak T, Ohkawara Y, Sallenave JM, Foley R, Sime PJ, et al. Gene transfer for cytokine functional studies in the lung: the multifunctional role of GM-CSF in pulmonary inflammation. J Leukoc Biol. 1996;59(4):481–8. [PubMed: 8613693]
41. Houzet L, Morello D, Defrance P, Mercier P, Huez G, and Kruys V. Regulated control by granulocyte-macrophage colony-stimulating factor AU-rich element during mouse embryogenesis. Blood. 2001;98(5):1281–8. [PubMed: 11520772]
42. Suzuki T, McCarthy C, Carey BC, Borchers M, Beck D, Wikenheiser-Brokamp KA, et al. Increased Pulmonary GM-CSF Causes Alveolar Macrophage Accumulation. Mechanistic Implications for Desquamative Interstitial Pneumonitis. Am J Respir Cell Mol Biol. 2020;62(1):87–94. [PubMed: 31310562]
43. Brooks SA, and Blackshear PJ. Tristetraprolin (TTP): interactions with mRNA and proteins, and current thoughts on mechanisms of action. Biochim Biophys Acta. 2013;1829(6–7):666–79. [PubMed: 23428348]
44. Carballo E, Lai WS, and Blackshear PJ. Evidence that tristetraprolin is a physiological regulator of granulocyte-macrophage colony-stimulating factor messenger RNA deadenylation and stability. Blood. 2000;95(6):1891–9. [PubMed: 10706852]
45. Taylor GA, Carballo E, Lee DM, Lai WS, Thompson MJ, Patel DD, et al. A pathogenetic role for TNF alpha in the syndrome of cachexia, arthritis, and autoimmunity resulting from tristetraprolin (TTP) deficiency. Immunity. 1996;4(5):445–54. [PubMed: 8630730]

46. Carballo E, and Blackshear PJ. Roles of tumor necrosis factor-alpha receptor subtypes in the pathogenesis of the tristetraprolin-deficiency syndrome. Blood. 2001;98(8):2389–95. [PubMed: 11588035]
47. Liu Q, Cheng LI, Yi L, Zhu N, Wood A, Changpriroa CM, et al. p47phox deficiency induces macrophage dysfunction resulting in progressive crystalline macrophage pneumonia. Am J Pathol. 2009;174(1):153–63. [PubMed: 19095958]
48. Feldmesser M, Kress Y, and Casadevall A. Intracellular crystal formation as a mechanism of cytotoxicity in murine pulmonary Cryptococcus neoformans infection. Infect Immun. 2001;69(4):2723–7. [PubMed: 11254641]
49. Guo L, Johnson RS, and Schuh JC. Biochemical characterization of endogenously formed eosinophilic crystals in the lungs of mice. J Biol Chem. 2000;275(11):8032–7. [PubMed: 10713123]
50. Ward JM. Pulmonary pathology of the motheaten mouse. Vet Pathol. 1978;15(2):170–8. [PubMed: 664185]
51. Ward JM, Yoon M, Anver MR, Haines DC, Kudo G, Gonzalez FJ, et al. Hyalinosis and Ym1/Ym2 Gene Expression in the Stomach and Respiratory Tract of 129S4/SvJae and Wild-Type and CYP1A2-Null B6,129 Mice. The American Journal of Pathology. 2001;158(1):323–32. [PubMed: 11141507]
52. Zhao J, Zhu H, Wong CH, Leung KY, and Wong WS. Increased lungkine and chitinase levels in allergic airway inflammation: a proteomics approach. Proteomics. 2005;5(11):2799–807. [PubMed: 15996009]
53. Chang NC, Hung SI, Hwa KY, Kato I, Chen JE, Liu CH, et al. A macrophage protein, Ym1, transiently expressed during inflammation is a novel mammalian lectin. J Biol Chem. 2001;276(20):17497–506. [PubMed: 11297523]
54. Lee CG, Da Silva CA, Lee JY, Hartl D, and Elias JA. Chitin regulation of immune responses: an old molecule with new roles. Curr Opin Immunol. 2008;20(6):684–9. [PubMed: 18938241]
55. Owhashi M, Arita H, and Hayai N. Identification of a novel eosinophil chemotactic cytokine (ECF-L) as a chitinase family protein. J Biol Chem. 2000;275(2):1279–86. [PubMed: 10625674]
56. Yousem SA, Colby TV, and Gaensler EA. Respiratory Bronchiolitis-Associated Interstitial Lung Disease and Its Relationship to Desquamative Interstitial Pneumonia. Mayo Clinic Proceedings. 1989;64(11):1373–80. [PubMed: 2593722]
57. Hellemons ME, Moor CC, von der Thusen J, Rossius M, Odink A, Thorgersen LH, et al. Desquamative interstitial pneumonia: a systematic review of its features and outcomes. Eur Respir Rev. 2020;29(156).
58. Malur A, Baker AD, McCoy AJ, Wells G, Barna BP, Kavuru MS, et al. Restoration of PPARgamma reverses lipid accumulation in alveolar macrophages of GM-CSF knockout mice. Am J Physiol Lung Cell Mol Physiol. 2011;300(1):L73–80. [PubMed: 21036914]
59. Guilliams M, De Kleer I, Henri S, Post S, Vanhoutte L, De Prijck S, et al. Alveolar macrophages develop from fetal monocytes that differentiate into long-lived cells in the first week of life via GM-CSF. J Exp Med. 2013;210(10):1977–92. [PubMed: 24043763]
60. Zaslona Z, Przybranowski S, Wilke C, van Rooijen N, Teitz-Tennenbaum S, Osterholzer JJ, et al. Resident alveolar macrophages suppress, whereas recruited monocytes promote, allergic lung inflammation in murine models of asthma. J Immunol. 2014;193(8):4245–53. [PubMed: 25225663]
61. Seymour JF, Presneill JJ, Schoch OD, Downie GH, Moore PE, Doyle IR, et al. Therapeutic efficacy of granulocyte-macrophage colony-stimulating factor in patients with idiopathic acquired alveolar proteinosis. Am J Respir Crit Care Med. 2001;163(2):524–31. [PubMed: 11179134]
62. Venkateshiah SB, Yan TD, Bonfield TL, Thomassen MJ, Meziane M, Czich C, et al. An open-label trial of granulocyte macrophage colony stimulating factor therapy for moderate symptomatic pulmonary alveolar proteinosis. Chest. 2006;130(1):227–37. [PubMed: 16840407]
63. Francisco-Cruz A, Aguilar-Santelises M, Ramos-Espinosa O, Mata-Espinosa D, Marquina-Castillo B, Barrios-Payan J, et al. Granulocyte-macrophage colony-stimulating factor: not just another haematopoietic growth factor. Med Oncol. 2014;31(1):774. [PubMed: 24264600]

64. Thomas RS, Tymms MJ, McKinlay LH, Shannon MF, Seth A, and Kola I. ETS1, NFkappaB and AP1 synergistically transactivate the human GM-CSF promoter. Oncogene. 1997;14(23):2845–55. [PubMed: 9190901]

65. Cakouros D, Cockerill PN, Bert AG, Mital R, Roberts DC, and Shannon MF. A NF-kappa B/Sp1 region is essential for chromatin remodeling and correct transcription of a human granulocyte-macrophage colony-stimulating factor transgene. J Immunol. 2001;167(1):302–10. [PubMed: 11418664]

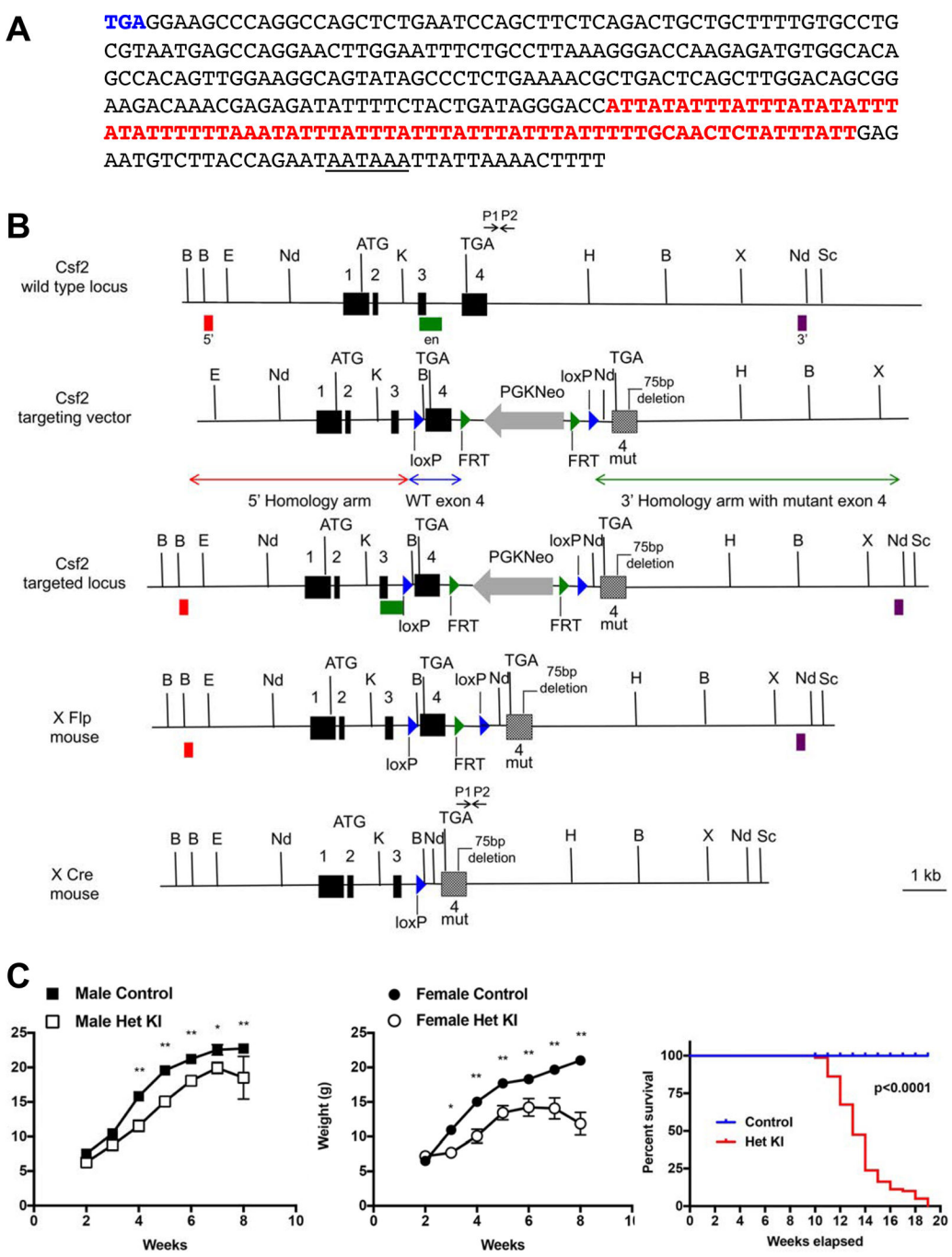

Figure 1. Generation and characterization of GM-CSFΔARE mice.

(A) The sequence of *Csf2* (GM-CSF) mRNA 3' UTR from the stop codon (blue) to the end of the transcript. The polyadenylation site is underlined, and the ARE sequence deleted in the mice is shown in red. (B) Schematic representation of the wild-type *Csf2* allele, the targeting vector, the targeted allele and the resulting alleles after either Flp or Cre recombination. The arrowheads show the FRT sites (green) and loxP sites (blue). The targeting vector contained the wild-type exon 4 as well as a mutant exon 4 with a 75 bp ARE deletion. Cre recombination results in the knock-in of the mutant exon 4. The red,

purple, and green boxes indicate the positions of the 5' probe, 3' probe, and *Neo* probe for Southern blot analysis, respectively. P1 and P2 indicate the sites for the genotyping PCR primers 1 (P1) and primer 2 (P2). B, BamHI; E, EcoRI; Nd, NdeI; K, KpnI; H, HindIII; X, XhoI; Sc, ScaI. (C) Growth curves for males (Control, n=7; Het KI, n=4; left) and females (Control, n=6; Het KI, n=4; middle). Kaplan Meier Survival Curves for control and Het KI mice (right). Results are the mean ± SEM. Statistical analysis of growth curves was determined using two-way ANOVA with Sidak's multiple comparison test (*$p<0.05$, **$p<0.01$). Survival curves were analyzed using the Mantel-Cox log-rank test.

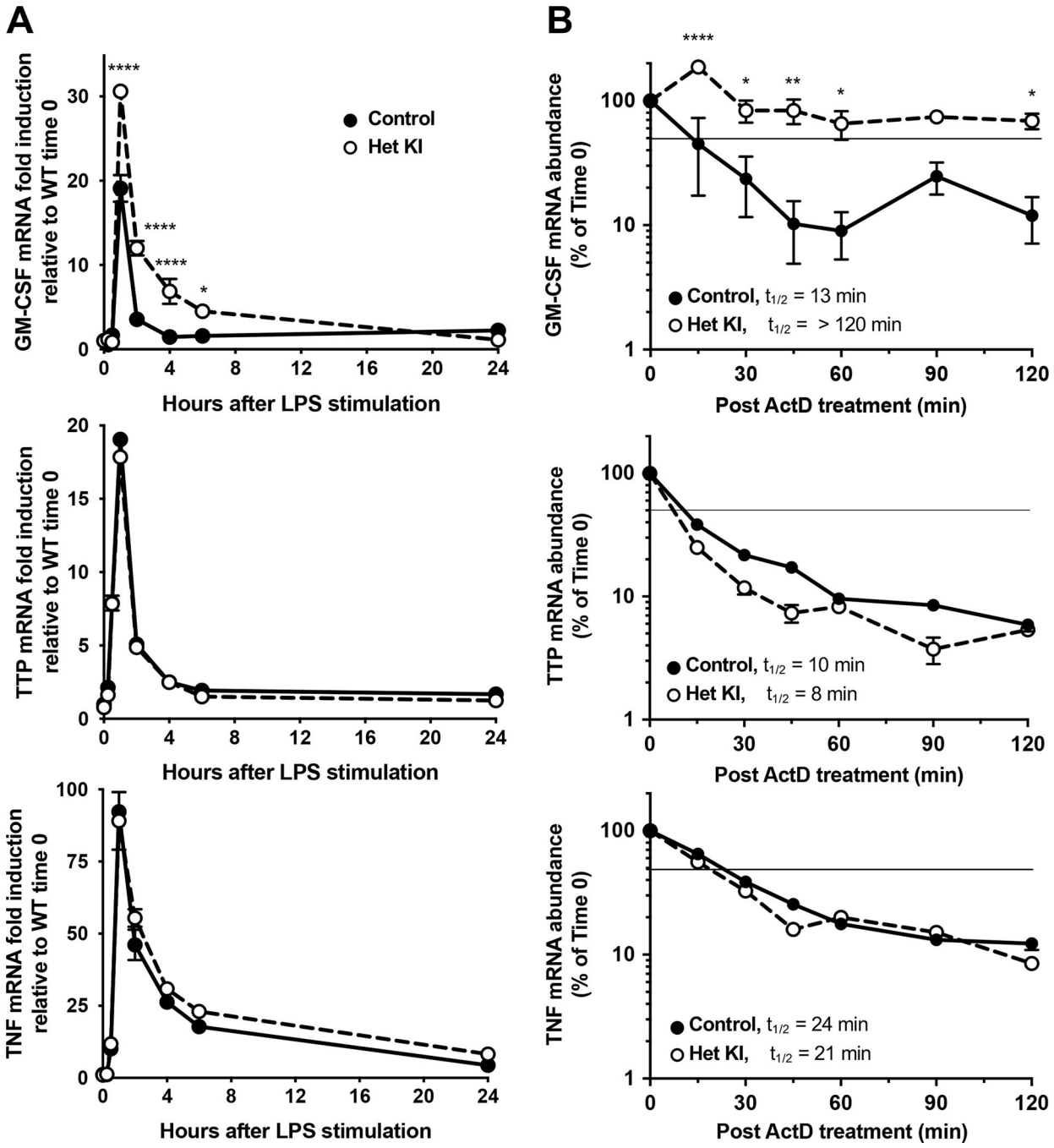

Figure 2. Enhanced mRNA stability after deletion of the GM-CSF 3'UTR ARE.

(A) Bone marrow-derived macrophages were treated with LPS (1 μg/ml), then RNA was extracted at the indicated time points. mRNA levels were determined by real-time PCR (normalized to β-actin). (B) Bone marrow-derived macrophages were stimulated with LPS (1 μg/ml) for 1 h and then treated with Actinomycin D (ActD; 5 μg/ml) to stop transcription. *Csf2* transcript abundance was determined by real-time PCR (normalized to β-actin), and is expressed as a percentage of the abundance at time zero (before the addition of ActD). The profiles of *Zfp36* (TTP) and *Tnf* mRNAs are shown in the middle and bottom panels,

respectively. Note that the Y-axis for mRNA abundance is shown in a log scale. The horizontal line indicates 50% of the original mRNA level. Results shown are the means ± SEM, and statistical significance was determined using a two-way ANOVA with Sidak's multiple comparison test (*p<0.05, **p< 0.01, ****p<0.0001). The approximate half-lives ($t_{1/2}$) of mRNAs in each genotype are indicated for each graph.

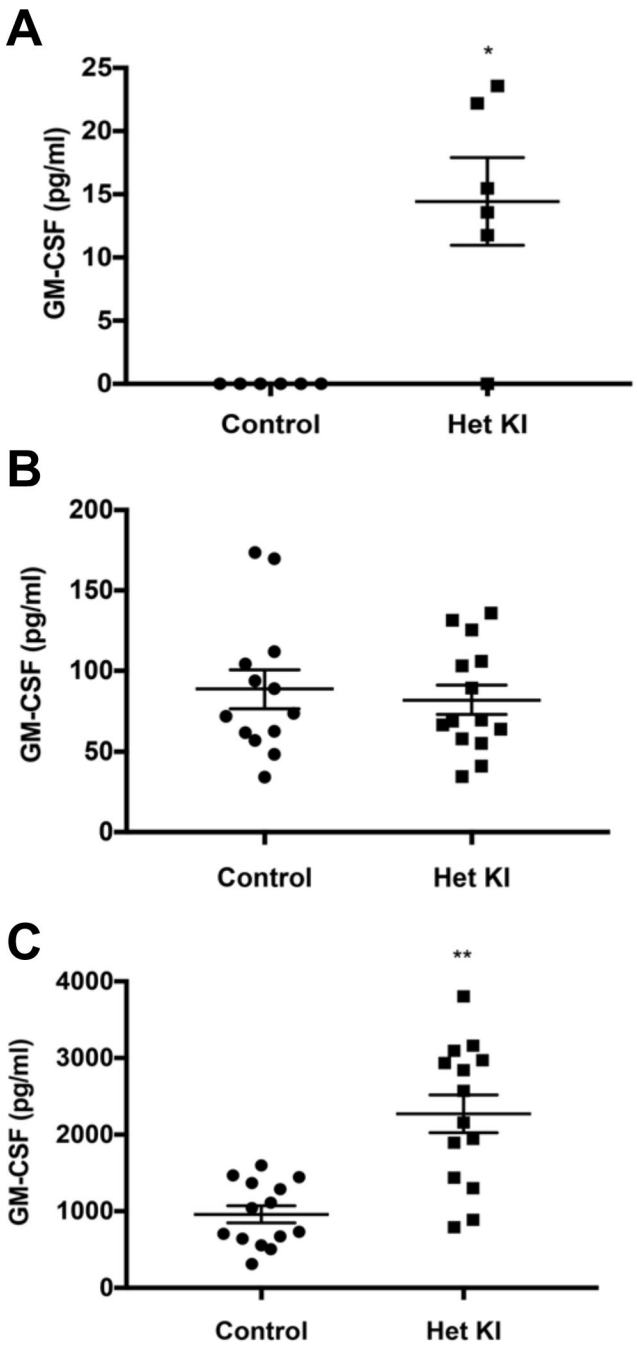

Figure 3. Increased production of GM-CSF in serum and lung from the GM-CSFΔARE mice.

GM-CSF protein levels in 8–12 week-old mice were analyzed by ELISA. (A) Serum; control (n=6, 2 males and 4 females), Het KI (n=6, 3 males and 3 females). (B) Bronchoalveolar lavage (BAL) fluid; control (n=13, 7 males and 6 females), Het KI (n=14, 6 males and 8 females). (C) Lung homogenates; control (n=14, 7 males and 7 females), Het KI (n=15, 7 males and 8 females). Statistical analysis was determined using unpaired Student's t tests with Welch's correction (*$p<0.05$, ** $p<0.01$).

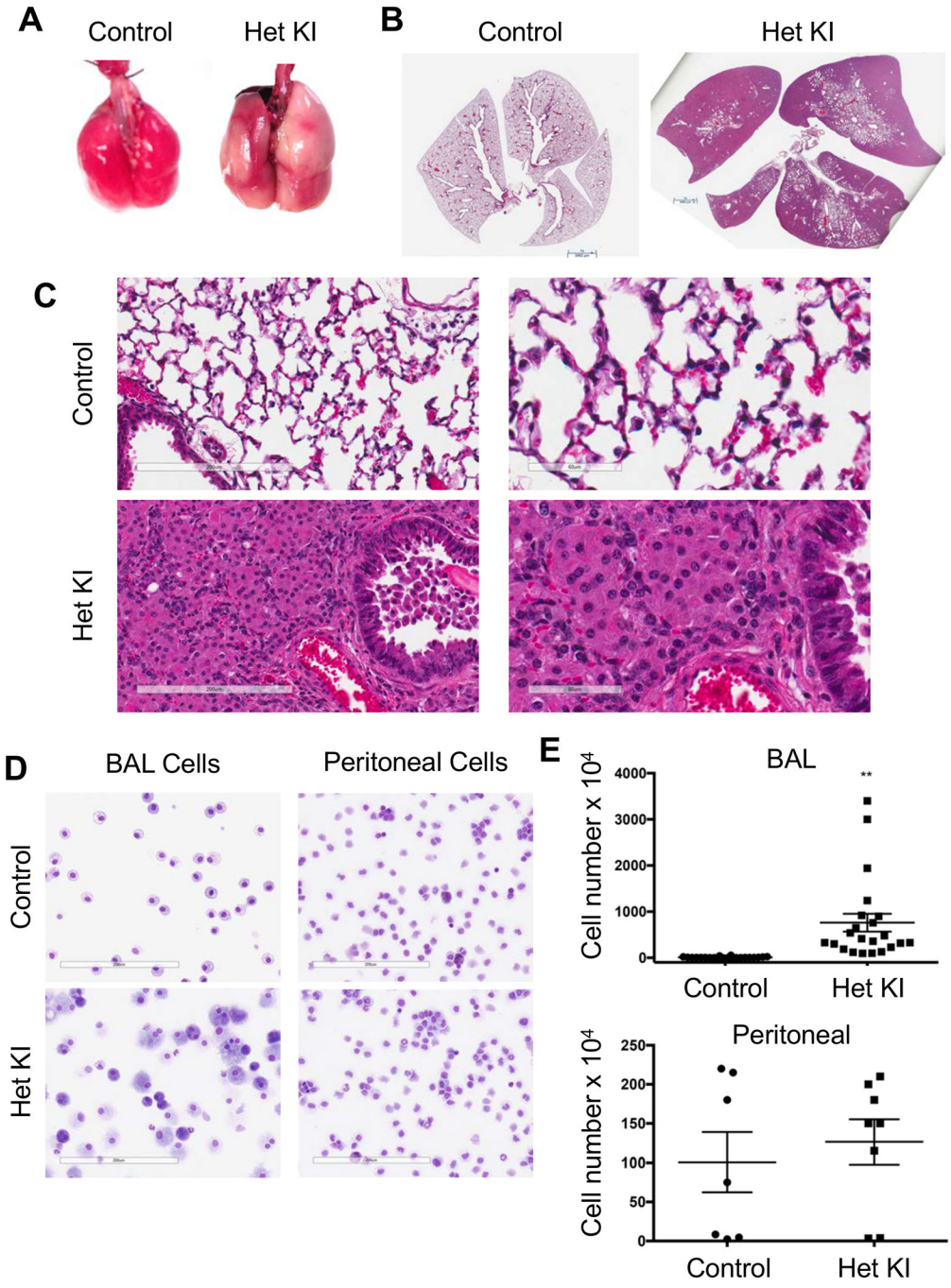

Figure 4. Lung phenotype of GM-CSFΔARE mice.

(A) Photographs of lungs from control (9 week-old female) and Het KI (9 week-old male) mice. The control lung was inflated with formalin before photography. (B) Gross view of hematoxylin and eosin-stained lung sections (control, 10 week-old female; Het KI, 10 week-old male). (C) Hematoxylin and eosin-stained sections of lungs from control and Het KI mice at low (20x; left) and high (40x; right) magnification. (D) Wright's stain of BAL fluid (control, 12 week-old male; Het KI, 12 week-old female) and peritoneal cells (control, 12 week-old male; Het KI, 12 week-old male). (E) Cell numbers of BAL fluid (10 control,

5 males and 5 females; 12 Het KI, 5 males and 7 females) and peritoneal cells (7 control, males and females; 8 Het KI, males and females). Data are shown in a scatter plot with mean ± SEM. Statistical analysis was performed using unpaired Student's t tests with Welch's correction (**$p<0.01$).

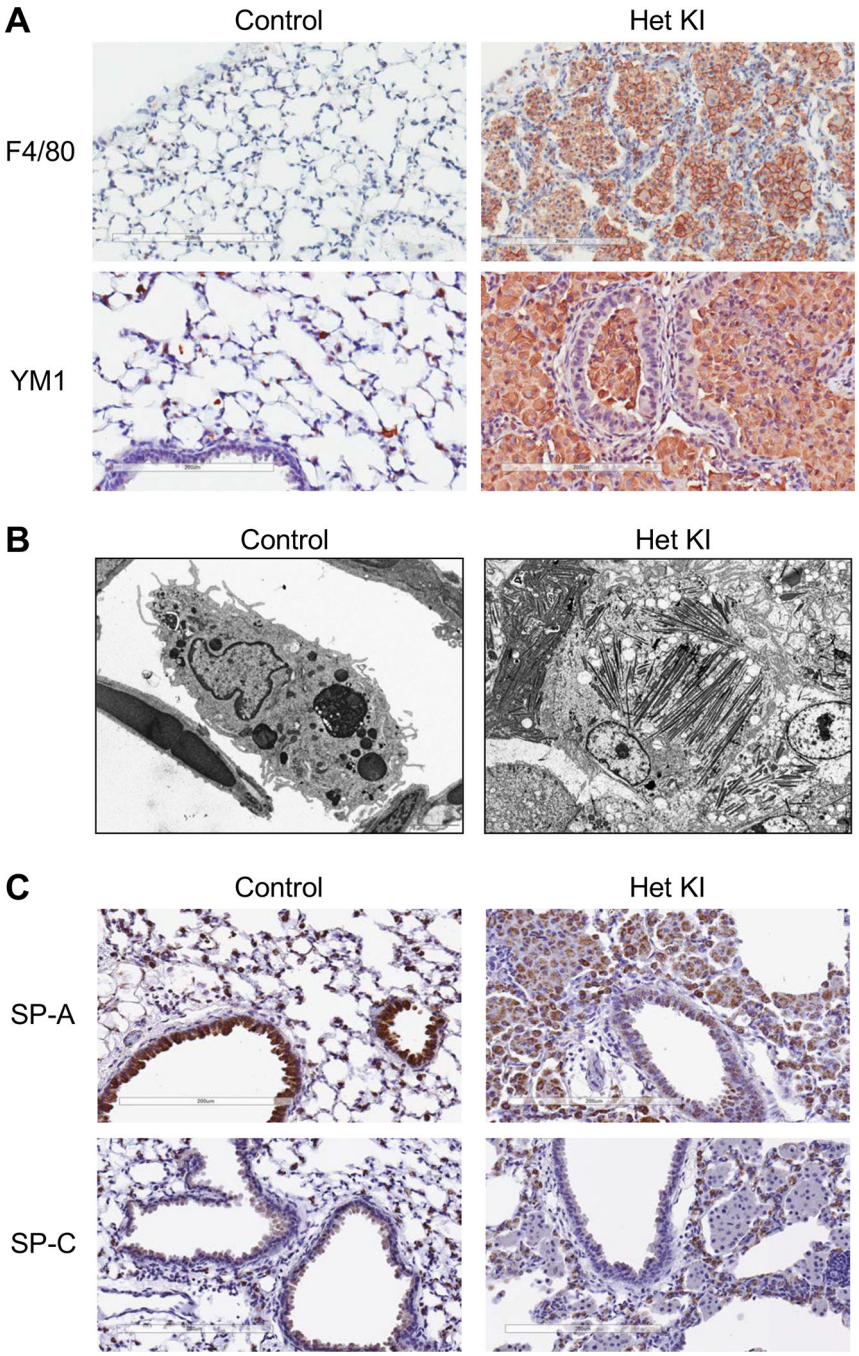

Figure 5. Immunostaining of lungs from GM-CSFΔARE mice.

(A) Control and Het KI lung sections were immunostained for F4/80 (control, 10 week-old male; Het KI, 10 week-old male) and Ym1 (control, 9 week-old female; Het KI, 9 week-old male). Results are shown at 20x magnification. (B) Ultrastructural analysis of lungs from control (12 week-old male) and Het KI (12 week-old male) mice. (C) Immunostaining of lungs from control (10 week-old male) and Het KI (10 week-old male) mice with surfactant-associated proteins SP-A and SP-C. Results are shown at 20x magnification.

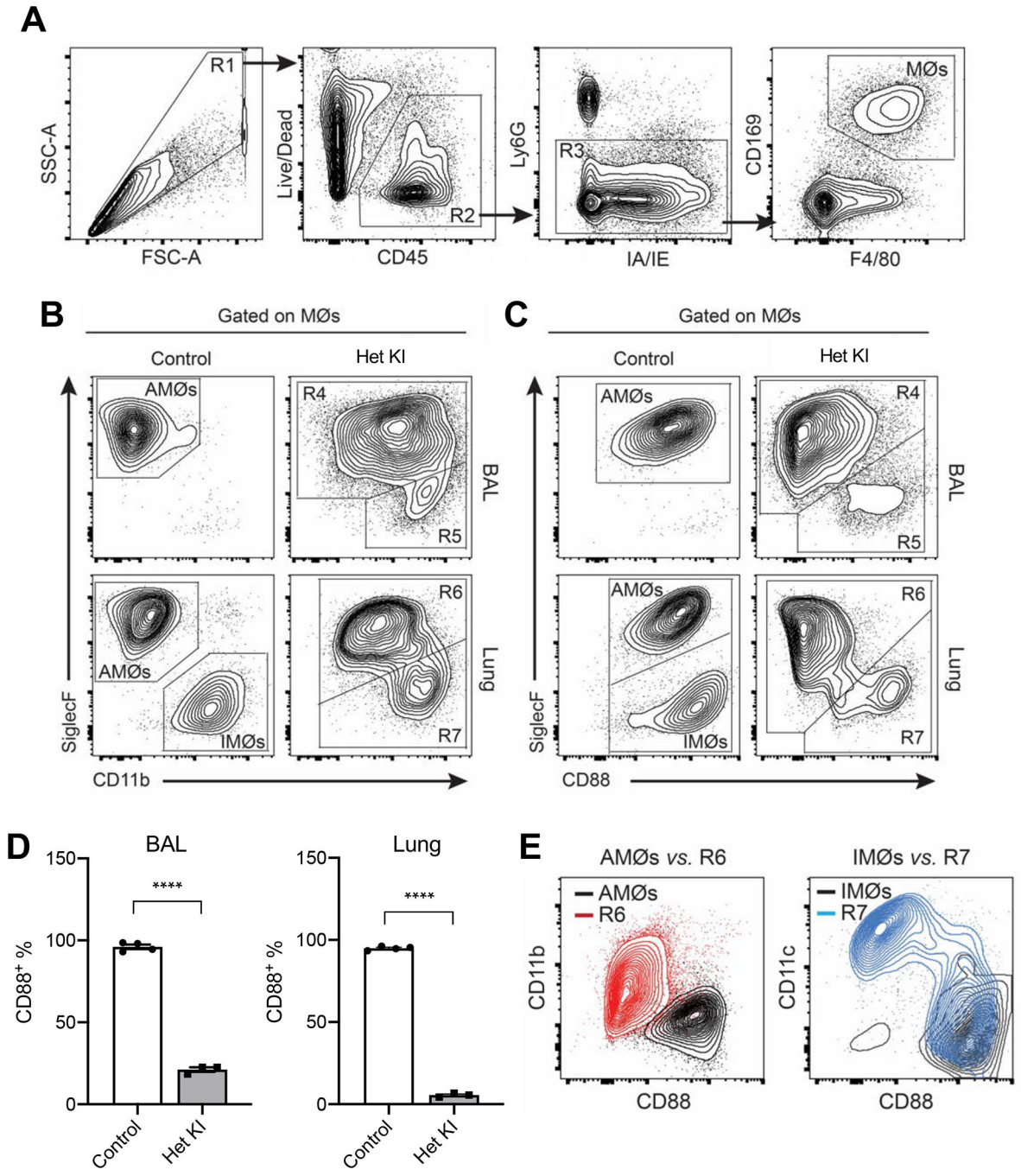

Figure 6. Characteristics of pulmonary alveolar macrophages from GM-CSFΔARE mice.

(A) Gating strategy to identify pulmonary macrophages from male and female mice at 12 weeks of age. R1 identifies singlets; R2 identifies live $CD45^+$ immune cells; R3 excludes neutrophils from immune cells (non-neutrophils); MØs = macrophages ($CD169^+F4/80^+$). (B) The cells within the MØ gate in Panel A were sorted with SiglcF and CD11b. Representative results are shown. (C) The cells within the MØ gate in Panel A were sorted with SiglcF and CD88. Representative results are shown. AMØs = alveolar macrophages ($SiglecF^+CD11b^-CD88^+$), IMØs = pulmonary interstitial

macrophages (SiglecF^{-}CD11b^{+}CD88^{+}). R4 and R6 = AMØ-like cells, R7 = IMØ-like cells, R5 = SiglecF^{-}CD11b^{+} cells. (D) The proportion of CD88 expressing AMØs (Control, n=4) and R4 (Het KI, n=3) in BAL fluid (left); CD88 expressing AMØs (Control, n=4) and R6 (Het KI, n=3) in lungs (right). The data are shown as a scatter plot with mean ± SEM. Statistical analysis was performed using unpaired Student's t tests with Welch's correction (****$p<0.0001$). (E) Comparisons are shown between AMØs and R6 (left), and between IMØs and R7 (right).

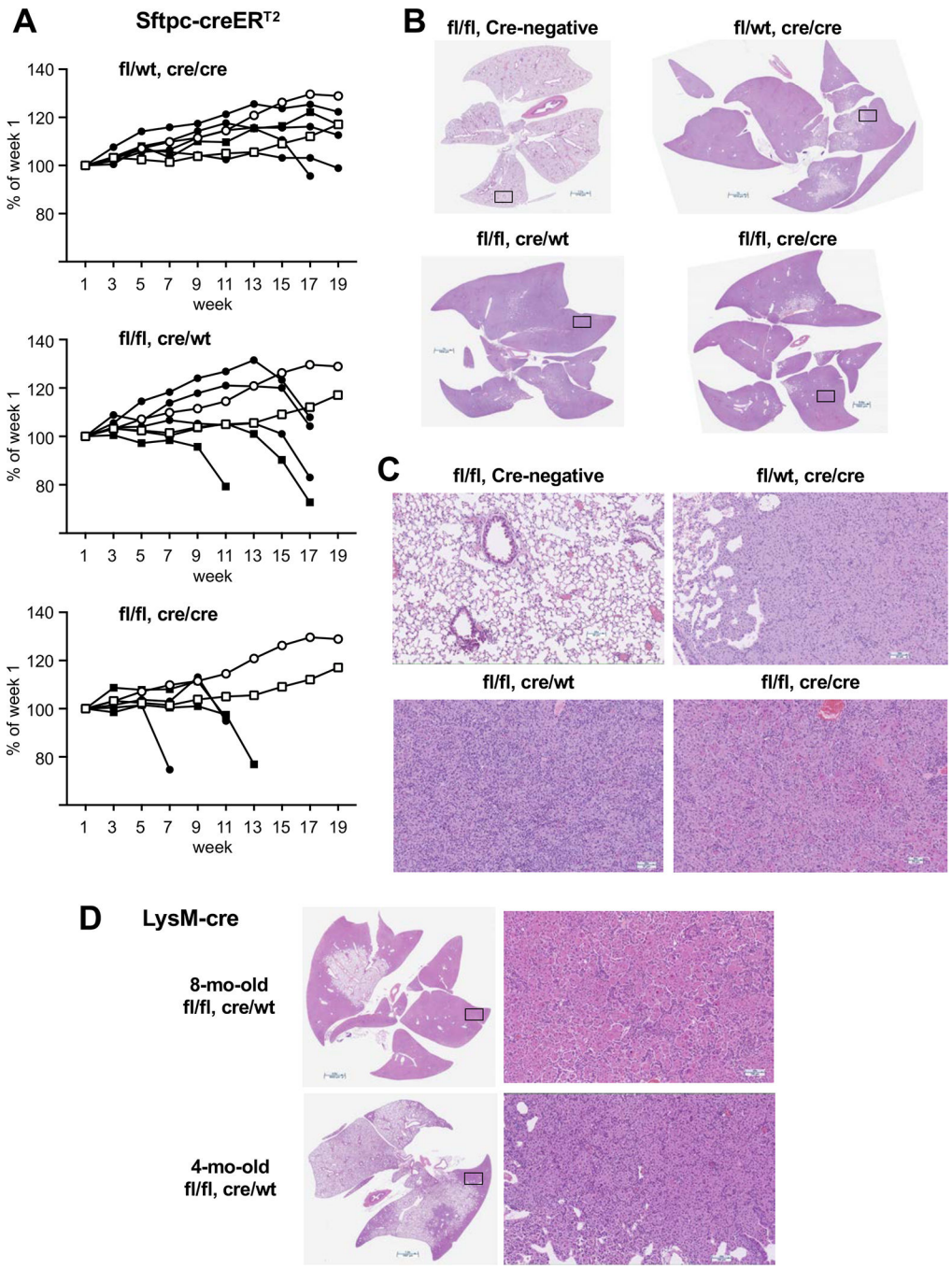

Figure 7. Phenotypes of tamoxifen-treated AT2 cell-specific GM-CSFΔARE mice and myeloid cell-specific GM-CSFΔARE mice.

(A) Growth curves. Tamoxifen-treated mice were monitored for 19 weeks after tamoxifen treatment. They were euthanized when they began exhibiting body weight loss and respiratory distress. The results are shown as percentages of each mouse's week 1 body weight; the circles indicate males, and the squares indicate females. The top panel shows *Csf2*$^{flARE/+}$ mice with homozygous Sftpc-creER^{T2} (fl/wt, cre/cre) (n=5, 4 males and 1 female); the middle panel shows *Csf2*$^{flARE/flARE}$ mice with heterozygous Sftpc-creER^{T2} (fl/fl, cre/wt) (n=5, 3 males and 2 females); and the bottom panel shows *Csf2*$^{flARE/flARE}$

mice with homozygous Sftpc-creER^{T2} (fl/fl, cre/cre) (n=4, 2 males and 2 females). As controls, fl/fl, Cre-negative mice are shown in each panel (open circles indicate an average of 6 males, and the open square indicates 1 female). (B) Representative hematoxylin and eosin-stained lungs from mice of each genotype after euthanasia. Panels show lung samples from an fl/fl Cre-negative male, an fl/wt cre/cre male, an fl/fl cre/wt female, and an fl/fl cre/cre male. The box in the picture indicates the area showed in the magnification. (C) Histology of lungs from mice of each genotype. The sections are shown at 20x magnification. (D) Representative hematoxylin and eosin-stained lung sections from *Csf2*$^{flARE/flARE}$ mice with heterozygous LysM-cre (fl/fl, cre/wt; males) at 8 months and 4 months of age. The left panels show the gross view of the lung sections. The box in the picture indicates the area that was magnified. The right panels show the 20x magnification view.

Table 1.

Analysis of transcripts involved in lipid metabolism, surfactant homeostasis, and alveolar macrophage development in lungs and AM from GM-CSFΔARE mice.

Gene	Het KI lung		p-value	Het KI AM		p-value
Csf2 (GM-CSF)	up	3.8	0.029	up	14	0.029
Abca3	nc	-		up	15.5	0.021
Cd36	down	54.5	0.022	nc	-	
Cyp27A1	down	3.2	0.003	nc	-	
Fapb1	up	4.2	0.137	down	107.7	0.014
Adgrf5 (Gpr116)	down	13.9	0.019	No expression		
Sftpa1	down	2.5	0.027	nc	-	
Sftpc	down	7.2	0.015	nc	-	
Nr1h3 (LXRa)	nc	-		up	7.6	0.035
Nr1h2 (LXRb)	nc	-		up	3.6	0.017
Pparg	nc	-		down	5.6	0.095
Spi1 (PU.1)	up	6.2	0.031	nc	-	
Itgam (Cd11b)	nc	-		up	30.4	0.003
Itgax (Cd11c)	up	9.1	0.083	up	18.4	0.023
Siglecf	nc	-		down	2.7	0.007

Lung and AM mRNA levels were measured by real-time RT-PCR in control and Het KI mice, using male and female mice of 8–12 weeks of age, as described in Methods.

Results were expressed as the ratios of control and Het KI average values, after internal normalization to *Actb* mRNA levels. Results shown for lung were from 4 control and 4 Het KI animals; results for AM were from 5 control (each control sample came from a pool of AM from 5 mice) and 6 Het KI mice. nc indicates no change in expression level when the $2^{-\Delta\Delta ct}$ value was 1. Statistical analysis was performed using unpaired Student's t tests with Welch's correction.

Table 2.

ELISA analysis of cytokines and chemokines in BAL fluid from GM-CSFΔARE mice.

Cytokine/Chemokine	Control (pg/ml)	Het KI (pg/ml)	p-value
m-CSF	0	39.5 ± 10.4	0.013
IL-6	0	68.1± 10.9	0.002
IFN-γ	3.9 ± 0.4	8.5 ± 1.4	0.02
MIP1α (CCL3)	5.7 ± 5.7	74.9 ± 16.6	0.007
MIP1β (CCL4)	4.6 ± 3.2	40.9 ± 8.9	0.024
KC (CXCL1)	11.3 ± 4.1	81.8 ± 11.7	0.001
IP10 (CXCL10)	3.1 ± 1.0	15.3 ± 2.3	0.002
Rantes (CCL5)	14.2 ± 2.4	22.6 ± 2.2	0.026
IL-17	0	0.82 ± 0.3	0.043

Cytokine and chemokine analyses were performed on BAL fluid collected from the mice at 8–12 weeks of age (control, n=6, 3 males and 3 females; HetKI, n=6, 3 males and 3 females), using the Millipore Sigma 25-plex mouse cytokine/chemokine magnetic bead panel. Results shown are mean ± SEM, and statistical analysis was performed using unpaired Student's t tests with Welch's correction.